Modulation of Protein *S*-Nitrosylation by Isoprene Emission in Poplar[1]

Elisa Vanzo, Juliane Merl-Pham, Violeta Velikova, Andrea Ghirardo, Christian Lindermayr, Stefanie M. Hauck, Jörg Bernhardt, Katharina Riedel, Jörg Durner, and Jörg-Peter Schnitzler*

Helmholtz Zentrum München, Research Unit Environmental Simulation (E.V., V.V., A.G., J.-P.S.), Institute of Biochemical Plant Pathology (C.L., J.D.), and Research Unit Protein Science (J.M.-P., S.M.H.), D–85764 Neuherberg, Germany; Institute of Plant Physiology and Genetics, Bulgarian Academy of Sciences, 1113 Sofia, Bulgaria (V.V.); and Institute for Microbiology, Ernst-Moritz-Arndt University, 17487 Greifswald, Germany (J.B., K.R.)

ORCID IDs: 0000-0002-3422-4083 (J.M.-P.); 0000-0001-8410-5624 (J.B.); 0000-0002-9825-867X (J.-P.S.).

Researchers have been examining the biological function(s) of isoprene in isoprene-emitting (IE) species for two decades. There is overwhelming evidence that leaf-internal isoprene increases the thermotolerance of plants and protects them against oxidative stress, thus mitigating a wide range of abiotic stresses. However, the mechanisms of abiotic stress mitigation by isoprene are still under debate. Here, we assessed the impact of isoprene on the emission of nitric oxide (NO) and the *S*-nitroso-proteome of IE and non-isoprene-emitting (NE) gray poplar (*Populus* × *canescens*) after acute ozone fumigation. The short-term oxidative stress induced a rapid and strong emission of NO in NE compared with IE genotypes. Whereas IE and NE plants exhibited under nonstressful conditions only slight differences in their *S*-nitrosylation pattern, the in vivo *S*-nitroso-proteome of the NE genotype was more susceptible to ozone-induced changes compared with the IE plants. The results suggest that the nitrosative pressure (NO burst) is higher in NE plants, underlining the proposed molecular dialogue between isoprene and the free radical NO. Proteins belonging to the photosynthetic light and dark reactions, the tricarboxylic acid cycle, protein metabolism, and redox regulation exhibited increased *S*-nitrosylation in NE samples compared with IE plants upon oxidative stress. Because the posttranslational modification of proteins via *S*-nitrosylation often impacts enzymatic activities, our data suggest that isoprene indirectly regulates the production of reactive oxygen species (ROS) via the control of the *S*-nitrosylation level of ROS-metabolizing enzymes, thus modulating the extent and velocity at which the ROS and NO signaling molecules are generated within a plant cell.

It has been demonstrated that isoprene protects plants against a plethora of abiotic stresses (Singsaas et al., 1997; Behnke et al., 2007; Velikova et al., 2008; Vickers et al., 2009b). Since the discovery of the positive influence of isoprene emission on plants' photosynthetic processes in the early 1990s (Sharkey and Singsaas, 1995), many efforts have been made to explain the primary mechanism of isoprene functioning. Most attention was given to the hypothesis that isoprene improves the thermotolerance of the photosynthetic machinery by stabilizing chloroplast (thylakoid) membranes during short, high-temperature episodes (Sharkey and Singsaas, 1995; Loreto and Schnitzler, 2010). Successive studies underlined that isoprene helps maintain high rates of chloroplastic electron transport and CO_2 assimilation during heat stress and accelerates recovery from stress (Singsaas and Sharkey, 2000; Velikova and Loreto, 2005; Velikova et al., 2006; Behnke et al., 2010b; Way et al., 2011).

One mechanistic explanation is that isoprene molecules are dissolved in thylakoid membrane and prevent membrane lipid denaturation following oxidative stress (Sharkey and Yeh, 2001). It was suggested that isoprene acts directly to stabilize the membrane (Sharkey and Yeh, 2001; Siwko et al., 2007). However, recent experiments with phosphatidylcholine liposomes showed that physiologically relevant intramembrane concentrations of isoprene do not alter membrane viscosity (Harvey et al., 2015). Nevertheless, Velikova et al. (2011) reported that, during high-temperature treatments, isoprene stabilized the macroorganization of the pigment-protein complexes of light-harvesting complex II in the thylakoid grana and that the disorganization of macroassemblies in isoprene-emitting (IE) chloroplasts began at higher temperatures compared

[1] This work was supported by the European Science Foundation Eurocores program EuroVOL within the joint research project MOMEVIP (to J.-P.S.) and by the Alexander von Humboldt Foundation (to V.V.).

* Address correspondence to jp-schnitzler@helmholtz-muenchen.de.

The author responsible for distribution of materials integral to the findings presented in this article in accordance with the policy described in the Instructions for Authors (www.plantphysiol.org) is: Jörg-Peter Schnitzler (jp-schnitzler@helmholtz-muenchen.de).

J.-P.S., C.L., and J.D. conceived the original research plan; C.L. and J.-P.S. supervised the experiments; E.V. and V.V. performed the experiments; J.M.-P., S.M.H., and A.G. provided technical assistance to E.V.; E.V., V.V., J.M.-P., J.B., K.R., and A.G. analyzed the data; E.V. wrote the article with contributions from all coauthors; J.-P.S. supervised and complemented the writing.

www.plantphysiol.org/cgi/doi/10.1104/pp.15.01842

with their nonemitting counterparts. Moreover, Velikova et al. (2011) showed decreased membrane permeability and more efficient primary photochemistry at PSII in IE plants at high temperatures (40°C–45°C). However, how isoprene contributes to this protection is still unknown.

The antioxidant hypothesis is the second mechanistic explanation by which isoprene may directly or indirectly exert its protective effect in plant cells. Plants that were fumigated with isoprene showed less visible ultrastructural (chloroplast) damage and less impairment of photosynthetic processes upon acute ozone fumigation than plants where isoprene was absent (Loreto et al., 2001). In conjunction with this hypothesis, leaf levels of hydrogen peroxide (H_2O_2; Loreto and Velikova, 2001; Behnke et al., 2010a), singlet oxygen (Affek and Yakir, 2002; Velikova, et al., 2004), and the free radical nitric oxide (NO; Velikova et al., 2005) were found to be lower in stressed plants when leaf internal isoprene was present. Taken together, these findings strongly indicate that endogenous isoprene modulates the oxidative and nitrosative load in plant tissue upon abiotic stress. However, the mechanism by which this modulation occurs remains unknown.

The generation of NO and reactive oxygen species (ROS; such as H_2O_2 and singlet oxygen) is a general plant response to many environmental stresses, such as acute ozone, drought, salinity, and heavy metals (Mahalingam et al., 2006; Rodríguez-Serrano et al., 2006; Pasqualini et al., 2009; Corpas et al., 2011; Noctor et al., 2014). Excess generation and accumulation of NO and ROS can cause modifications of cellular macromolecules such as nucleic acids and membrane lipids and proteins, thus leading to malfunctioning of enzymes and organelles, ultimately inducing cell death (Mittler, 2002). Even under optimal conditions, these compounds are produced continuously in primary plant metabolism as side products of the chloroplastic and mitochondrial electron transport chains (Foyer and Noctor, 2003). Cellular levels of ROS and NO are tightly regulated by an efficient antioxidant defense system composed of scavenging enzymes and a nonenzymatic barrier (Foyer and Noctor, 2003). In this context, isoprene may constitute a part of the nonenzymatic oxidative defense system (Vickers et al., 2009b) and may substitute for other antioxidants (Peñuelas et al., 2005; Behnke at al., 2009).

A more indirect mode of isoprene functioning is also under debate (for review, see Vickers et al., 2009a). Chloroplasts, the main targets of the proposed isoprene function(s), are a major source of NO (Jasid et al., 2006). It is suggested that endogenous NO in chloroplasts can exert either antioxidant or prooxidant effects on chloroplast macromolecules and influence the integrity of membrane processes (Jasid et al., 2006). NO can prevent in chloroplasts the Fenton reaction by scavenging iron, thus avoiding the formation of hydroxyl radicals (Wink et al., 1995), radicals that can be efficiently quenched by isoprene (Huang et al., 2011). Chloroplasts are also the main site of carbon and nitrogen metabolism and ROS production. Isoprene may modulate directly or indirectly the oxidative and nitrosative state of chloroplasts undergoing stress by modulating NO-related signaling pathways. Due to their lipophilic structure, it is probable that isoprene and NO converge inside plants, but to what extent the molecular dialogue between isoprene and NO can affect NO- and ROS-related signaling is unknown.

NO signaling regulates many plant development processes, such as stomatal closure (Neill et al., 2002), germination (Bethke et al., 2004), flowering (He et al., 2004), senescence (Guo and Crawford, 2005), and hormonal signaling (Simontacchi et al., 2013). NO signaling also plays a well-established role during plant-pathogen responses (Delledonne et al., 1998; Durner et al., 1998) and abiotic stress reactions (Corpas et al., 2011). The hypersensitive response upon pathogen invasion is an example of programmed cell death and shares many similarities with the plant ozone response (Sandermann et al., 1998). In both cases (biotic and abiotic elicitor), the activation of the hypersensitive response is associated with a burst of NO and ROS occurring in the same time range (Ahlfors et al., 2009).

NO exerts its signaling action by directly altering proteins through posttranslational modifications (PTMs; i.e. *S*-nitrosylation, metal nitrosylation, and Tyr nitration). *S*-Nitrosylation, the covalent binding of NO to the thiol side of protein-Cys residues to form nitrosothiols, is regarded as the most important PTM of NO signaling in plants (Moreau et al., 2010). The binding and removal of NO is not strictly an enzymatic process and depends strongly on the redox status of the cell (Lindermayr and Durner, 2009). However, the enzymatic removal of the NO group via denitrosylation has been reported (Benhar et al., 2009), ensuring the reversibility of the modification. *S*-Nitrosylation and denitrosylation events together form the *S*-nitrosylation pattern of a cell under physiological conditions, which may strongly change upon stress (Abat and Deswal, 2009; Ortega-Galisteo et al., 2012). The *S*-nitrosylation of enzymes can either inhibit or activate their functions (Astier et al., 2012). It has been suggested that *S*-nitrosylation is involved in the regulation of ROS level under abiotic stress (Ortega-Galisteo et al., 2012; Lindermayr and Durner, 2015) by targeting the ROS-metabolizing enzymes.

This work assesses the proposed mechanism of isoprene in modulating NO signaling. Because *S*-nitrosylation, the covalent binding of NO to Cys moieties, is the main method of NO signaling, we identified targets of *S*-nitrosylation in IE and non-isoprene-emitting (NE) gray poplar (*Populus* × *canescens*) plants using the biotin switch assay in conjunction with mass spectrometry. After taking an inventory of putative *S*-nitrosylated proteins in IE and NE gray poplar plants under nonstressful conditions, we applied short, acute, ozone stress-triggering changes in the NO emission and *S*-nitroso-proteome depending on the presence of isoprene.

RESULTS AND DISCUSSION

Whole-Proteome Analysis Highlights Some Alterations in the Protein Profile of NE Gray Poplar under Control Conditions

Liquid chromatography-tandem mass spectrometry (LC-MS/MS) identification and label-free quantitative analysis of unstressed leaf samples revealed some differences in global protein abundances between IE (wild type and empty vector [EV]) and NE (Ra1 and Ra2) genotypes (Fig. 1). We identified and quantified 2,025 proteins; among these, 1,388 proteins were identified with two or more unique peptides, and 1,071 of them could be quantified with two or more unique peptides. Globally, the differences in protein abundance between IE and NE samples were small (Fig. 1), with 97% of the proteins within a logarithmic fold change of ±1 (Fig. 1A). The largest, significant fold changes between IE and NE genotypes were observed for the terpenoid cyclase and, as expected, for the isoprene synthase (ISPS), the target of the RNA interference-mediated suppression of isoprene emission. Moreover, the Rubisco large chain, a 50S ribosomal protein, a ubiquinone biosynthesis protein, and the chloroplast inner membrane import protein Tic22 exhibited significantly lower expression in the NE genotype. A higher

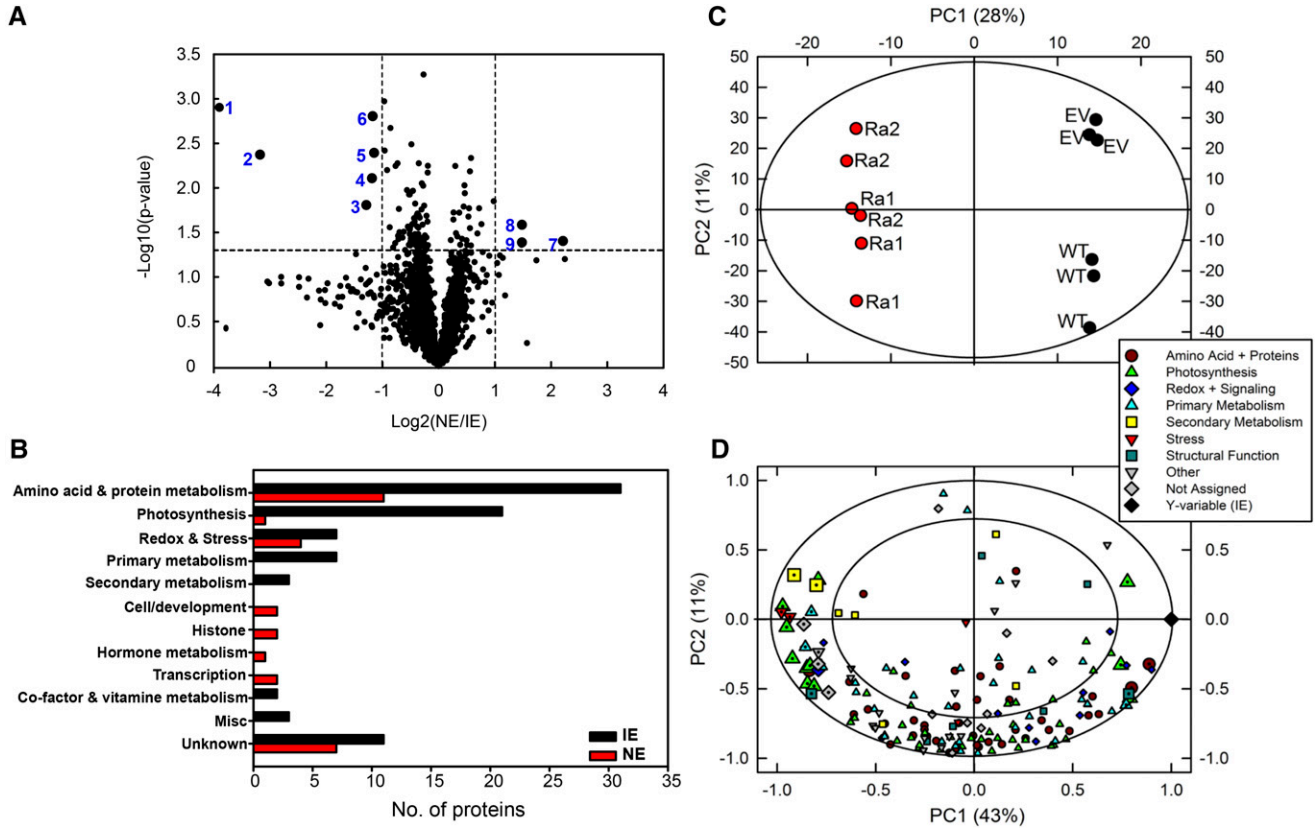

Figure 1. Whole-proteome comparison of IE (black) and NE (red) gray poplar leaves. A, Volcano plot showing the magnitude of differential protein abundance in NE and IE genotypes ($\log_2$ [fold change]) compared with the measure of statistical significance ($-\log_{10}$ [*P* value, Student's *t* test]). Vertical, dashed lines indicate log fold change of ±1, and the horizontal line indicates a significance value of $\alpha = 0.05$. The proteins with the highest and significant fold changes between NE and IE samples are highlighted and numbered as follows: 1 = terpenoid cyclase, 2 = isoprene synthase, 3 = Rubisco large chain, 4 = 50S ribosomal protein, 5 = ubiquinone biosynthesis protein, 6 = chloroplast inner membrane import protein Tic22, 7 = basic penta-Cys4, 8 = EP3-3 chitinase, and 9 = eukaryotic aspartyl protease family. B, Discriminant proteins that explain the separation between IE and NE gray poplar (116 in total; Supplemental Table S1) grouped according their functional categories. Black bars indicate up-regulated in IE samples and red bars indicate up-regulated in NE samples. C and D, Score (C) and loading (D) plots of OPLS of the whole proteome. PC, Principal component; WT, wild type. C, Plants were divided into the IE group (black circles; $n = 6$) and the NE group (red circles; $n = 6$). The ellipse indicates the tolerance based on Hotelling's t^2 with a significance level of 0.05. D, Each functional group of proteins is indicated with different colors. The outer and inner ellipses indicate 100% and 75% explained variance, respectively. Each point represents an independent plant in the score plot and an individual protein in the loading plot. OPLS model fitness is as follows: r^2 (*x*) = 69.9%, r^2 (*y*) = 100%, r^2 = 98.6%, and q^2 (cumulative) = 79.3% using one predictive component. RMSEE (root mean square error of estimation) = 0.072 and RMSEcv (root mean square error of cross validation) = 0.227. $P < 0.05$, cross-validated ANOVA.

expression was observed for the basic penta-Cys4, the EP3-3 chitinase, and the eukaryotic aspartyl protease family protein (Fig. 1A).

The orthogonal partial least square (OPLS) method was employed to dissect the differences between the IE and NE genotypes (Fig. 1, B–D). Among 116 discriminant proteins able to discriminate between IE and NE genotypes, 31 proteins were higher expressed and 85 proteins were lower expressed in the NE genotype, compared with the IE genotype (Supplemental Table S1).

Proteins with a higher abundance in the NE genotype comprised 11 enzymes that are involved in protein degradation (e.g. subtilase, Ser protease, and ubiquitin family protein) and protein folding (HEAT SHOCK PROTEIN70 [HSP70]). This increase in the NE genotype may be indicative of a substantial increase in protein degradation in this genotype. Two other more expressed proteins in the NE genotype are related to histones (winged-helix DNA-binding transcription factor and histone superfamily protein). This observation fits with the strong expression of histones in the chloroplast proteome of NE plants (Velikova et al., 2014). NE samples also showed a higher abundance of proteins involved in the stress response. These are the germin-like protein (+0.4) and the EP3-3 chitinase. The germin-like proteins have, besides their action in plant development, a proposed role in the plant defense response (Lane, 2002). The expression of these proteins is induced upon various biotic and abiotic stresses, and overexpression of the germin-like proteins enhanced the resistance against powdery mildew in barley (*Hordeum vulgare*; Zimmermann et al., 2006). Similarly, various biotic and abiotic stresses can induce the expression of plant chitinases (Kasprzewska, 2003). They catalyze the hydrolysis of β-1,4-bonds in chitin and are classified as PR proteins (e.g. EP3 chitinase from carrot [*Daucus carota*] is involved in programmed cell death [PCD]; Kasprzewska, 2003). Interestingly, each line had a specific proteome pattern, suggesting that the genetic transformation process can affect the whole proteome and cause off-target effects (Day et al., 2000; Latham et al., 2006).

For the visualization of the proteomic differences between lines and treatments, we applied Voronoi Treemaps (Figs. 2, 4, and 6) as introduced by Bernhardt et al. (2009). The major difference in the protein profiles of NE and IE plants (Fig. 2) was the lower abundance of several proteins in the NE genotype mostly involved in the light and dark reactions of photosynthesis. By contrast, only one protein related to photosynthesis was more abundant in the NE genotype (i.e. ferredoxin reductase). The reduction in protein content comprises subunits of the PSI and PSII complexes (e.g. oxygen-evolving complex, PSII assembly factor, and thylakoid luminal proteins), the cytochrome b_6f complex, ATP synthase, and the large chain of Rubisco, confirming the proteomic survey of IE and NE poplar chloroplasts (Velikova et al., 2014). It might be speculated that NE plants have a lower demand for components of the photosynthetic apparatus and also for the supply of chlorophyll, because several enzymes of the tetrapyrrole biosynthesis pathway that generate essential compounds, such as chlorophyll and heme (Tanaka et al., 2011), also are strongly reduced in concentration in the NE genotype. The lower amount of protein members of the photosynthetic apparatus may influence the physiology of NE poplar under unstressed conditions and upon stress. While initial physiological measurements showed no significant differences in the net CO_2 assimilation rates of both genotypes (Behnke et al., 2007, 2009, 2010a), recent observations reported lower gas exchange (Way et al., 2013) and electron transport rates (Velikova et al., 2015) in the NE genotype compared with the IE genotype.

In accordance with previous observations (Velikova et al., 2014), the down-regulation of antioxidant enzymes in the NE genotype can be confirmed at the cellular proteome level. The down-regulated enzymes are three different ascorbate peroxidase (APX) isoforms, superoxide dismutase (SOD), the glutathione *S*-transferase F11, and the monodehydroascorbate reductase (Fig. 2). The levels and activities of APX and SOD often correlate, and coordinated increases in either gene expression have been shown to improve tolerance to oxidative stress in cassava (*Manihot esculenta*; Xu et al., 2014). Due to the lower setting of several antioxidant enzymes in NE plants, the strict control of ROS production could be deregulated, explaining the higher in vitro accumulation of H_2O_2 in NE leaves upon high light and temperature treatment (Behnke et al., 2010a).

Overall, the proteomic characterization of IE and NE cell extracts from unstressed poplar shows that knockdown of the ISPS enzyme results in a distinct cellular and chloroplastic (Velikova et al., 2014) rearrangement of proteins and enzymes involved in photosynthetic processes, glycolysis and the tricarboxylic acid cycle, redox regulation, and protein translation (Fig. 2).

Isoprene Suppression Results in Slight Modification of the *S*-Nitroso-Proteome of Gray Poplar Plants under Unstressed Conditions

Similar to the overall proteomic survey, a label-free LC-MS/MS approach was applied to quantitatively compare the *S*-nitroso-proteome of the IE and NE genotypes in control conditions and immediately following the short, acute ozone exposure (next section). In total, 203 *S*-nitrosylated proteins were identified (Supplemental Table S2) after biotin switch and subsequent pull down.

Globally, IE and NE plants exhibited only minor differences in the *S*-nitrosylation pattern of unstressed plants (Supplemental Table S3). Five of these discriminant proteins were found to be more *S*-nitrosylated in NE plants (Supplemental Table S3; Fig. 6B). These are Rubisco activase, α-*N*-arabinofuranosidase (ARA), phosphoribulokinase (PRK), HSP70, and *O*-acetylserine(thiol)lyase (OAS-TL). By contrast, only one protein, a PSII assembly protein, was less *S*-nitrosylated in the NE genotype compared with the IE genotype.

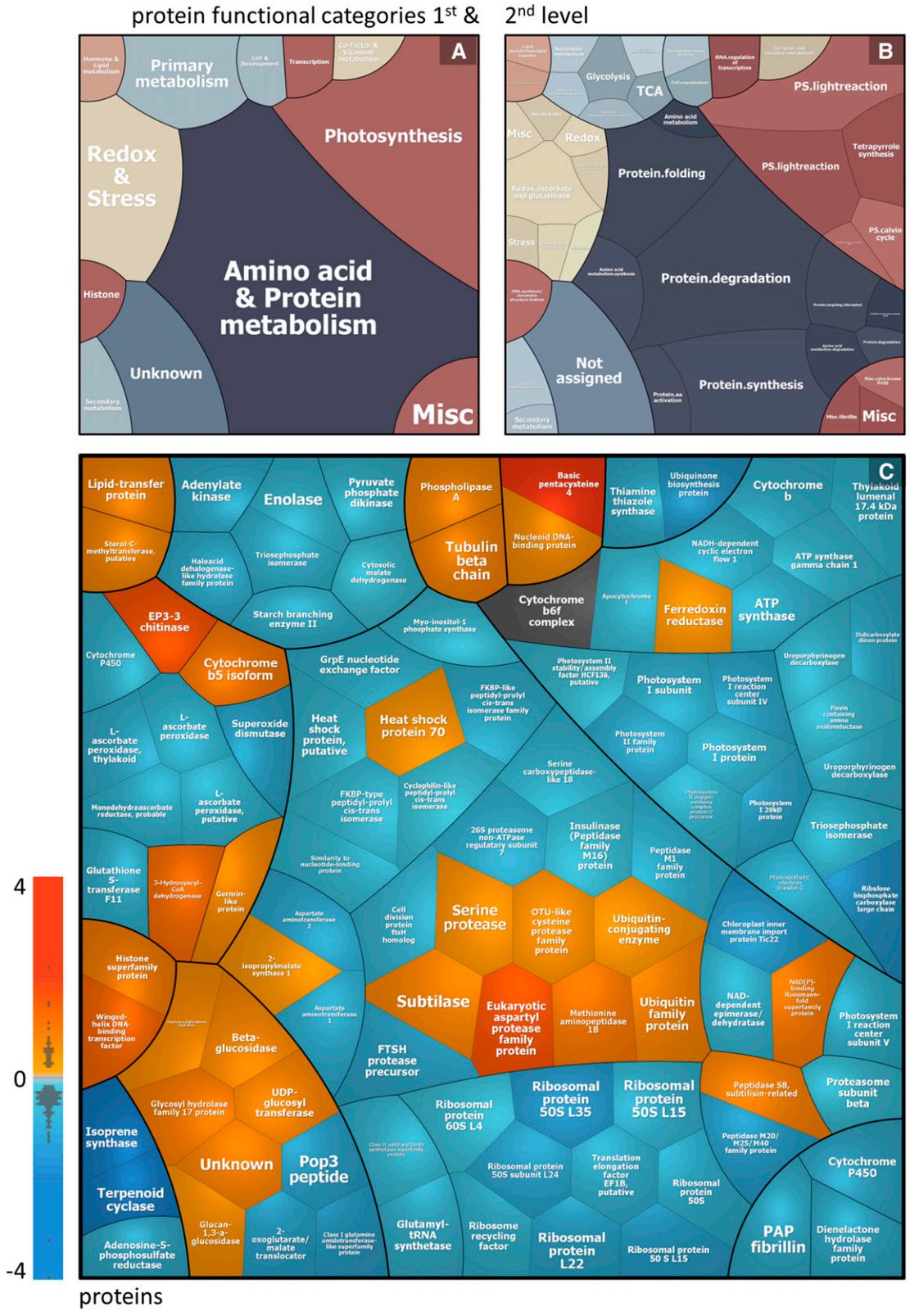

Figure 2. Voronoi Treemaps showing the overall proteome changes of IE (wild type and EV) and NE (Ra1 and Ra2) gray poplar leaves. The Treemaps subdivide the two-dimensional plane into subsections according to the hierarchical data structure of gene functional assignments, taken from the corresponding Arabidopsis orthologs (http://www.arabidopsis.org/tools/bulk/go/index.jsp), which were obtained via the POPGENIE (http://www.popgenie.org) database. A and B, Protein expression changes are

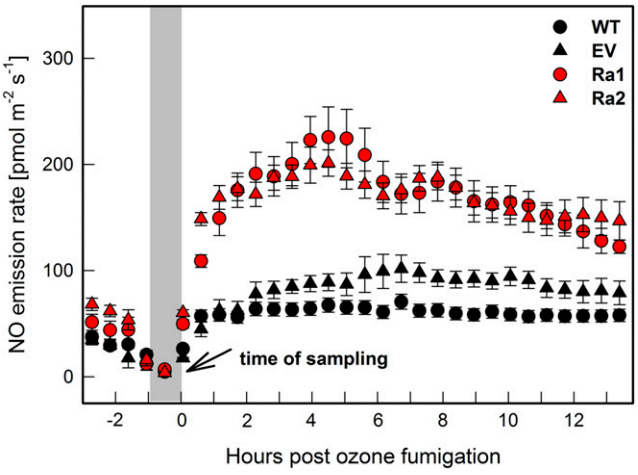

Figure 3. Time-course curves of NO emission rates in shoots of IE (wild type [WT] and EV) and NE (Ra1 and Ra2) gray poplar before and after ozone fumigation (800 nL L^{-1} for 1 h). Measurements were performed at 25°C and 500 μmol m^{-2} s^{-1} photosynthetic photon flux density. Values are means of four biological replicates ± SE. The vertical gray bar indicates the period of ozone fumigation.

Rubisco activase and PRK, two important enzymes in CO_2 fixation, are known targets of several redox-based PTMs (i.e. *S*-nitrosylation, Tyr nitration, and glutathionylation; Lindermayr et al., 2005; Lozano-Juste et al., 2011; Tanou et al., 2012), showing that a strong overlap in the signaling pathways of different PTMs exists and that the Calvin-Benson-Bassham (CBB) cycle is strongly redox regulated (Michelet et al., 2013). Interestingly, Rubisco activase is crucial not only for the maintenance of the high Rubisco activation state (Portis, 2003) but also for the photosynthetic light reactions, because the knockdown of Rubisco activase leads to a slower electron transport rate and a decrease in the content of PSII components (Cai et al., 2010). With regard to the reduction of electron transport rate and the content of PSII proteins in NE chloroplasts (Velikova et al., 2014), the higher proportion of constitutive *S*-nitrosylated Rubisco activase and PRK may be related functionally to these alterations. However, no functional characterization of *S*-nitrosylation/denitrosylation events in the enzyme activities of Rubisco activase and PRK has been reported thus far.

The *S*-nitrosylation of ARA was described recently (Vanzo et al., 2014). ARA hydrolyses the cleavage of terminal arabinofuranosyl residues from the pectin matrix and is involved in secondary cell wall biogenesis in hybrid aspen (*Populus tremula* × *Populus tremuloides*; Aspeborg et al., 2005).

OAS-TL, catalyzing the last step in Cys biosynthesis and sulfur assimilation, has one predicted *S*-nitrosylation site (Supplemental Table S2), but whether *S*-nitrosylation/denitrosylation impacts enzyme functionality is unknown. Notably, Alvarez et al. (2011) demonstrated that Tyr nitration, another route of NO signaling (Corpas et al., 2009), inhibits the enzymatic activity of OAS-TL.

HSP70 is a prominent target of *S*-nitrosylation in plants (Lindermayr et al., 2005; Abat and Deswal, 2009). HSP accumulation in response to heat stress has been reported (Kotak et al., 2007), and there is evidence that NO and H_2O_2 act as signals that promote the gene expression of HSPs under thermal stress (Volkov et al., 2006). Whether the higher degree of *S*-nitrosylation of HSP70 in NE plants is functionally related to the higher thermal sensitivity (Behnke et al., 2007, 2010b) of this genotype requires further analysis.

Acute Ozone Fumigation Stimulates NO Emission and Modifies the *S*-Nitroso-Proteome of IE and NE Gray Poplar

NO Emissions of IE and NE Gray Poplar following Acute Ozone

Under control conditions, emissions of NO did not differ significantly between NE and IE poplar genotypes, although a tendency to higher emission from the NE genotype was observed (Fig. 3). Emissions of NO were induced rapidly after the ozone exposure in both genotypes, but NO emissions were much more induced in NE shoots. In both genotypes, NO emissions reached maximal rates after approximately 3.5 h of ozone treatment. In the NE genotype, NO emission rates remained high until 7 h post ozone exposure. In contrast, the NO emissions in the IE genotype started to decline after the maximum, finally reaching almost similar rates to that before the ozone treatment. In NE plants, NO emission rates also decreased, but they still showed doubled intensities at the end of the observation period compared with the initial conditions. Such a difference in NO emission between different isoprene-emitter types is supported by previous results showing a stronger stimulation of NO emission in *Populus nigra* leaves with chemically inhibited isoprene emission exposed to oxidative stress (Velikova et al., 2008). An inverse correlation between isoprene emission and NO production also was observed in ozonized reed (*Phragmites australis*) leaves (Velikova et al., 2005). The finding that NE poplar emits significantly higher rates of NO upon ozone fumigation compared with the natural IE genotype is an indication that isoprene

Figure 2. (*Continued.*)
displayed according to their functional categories, and hierarchically structured functional assignments are displayed in Treemaps. C, Expression changes (log_2 ratios of condition 1 versus condition 2) were color coded: orange indicates increased in the NE genotype (log_2 ratio 4), gray indicates unchanged, and blue indicates decreased in the NE genotype (log_2 ratio 4).

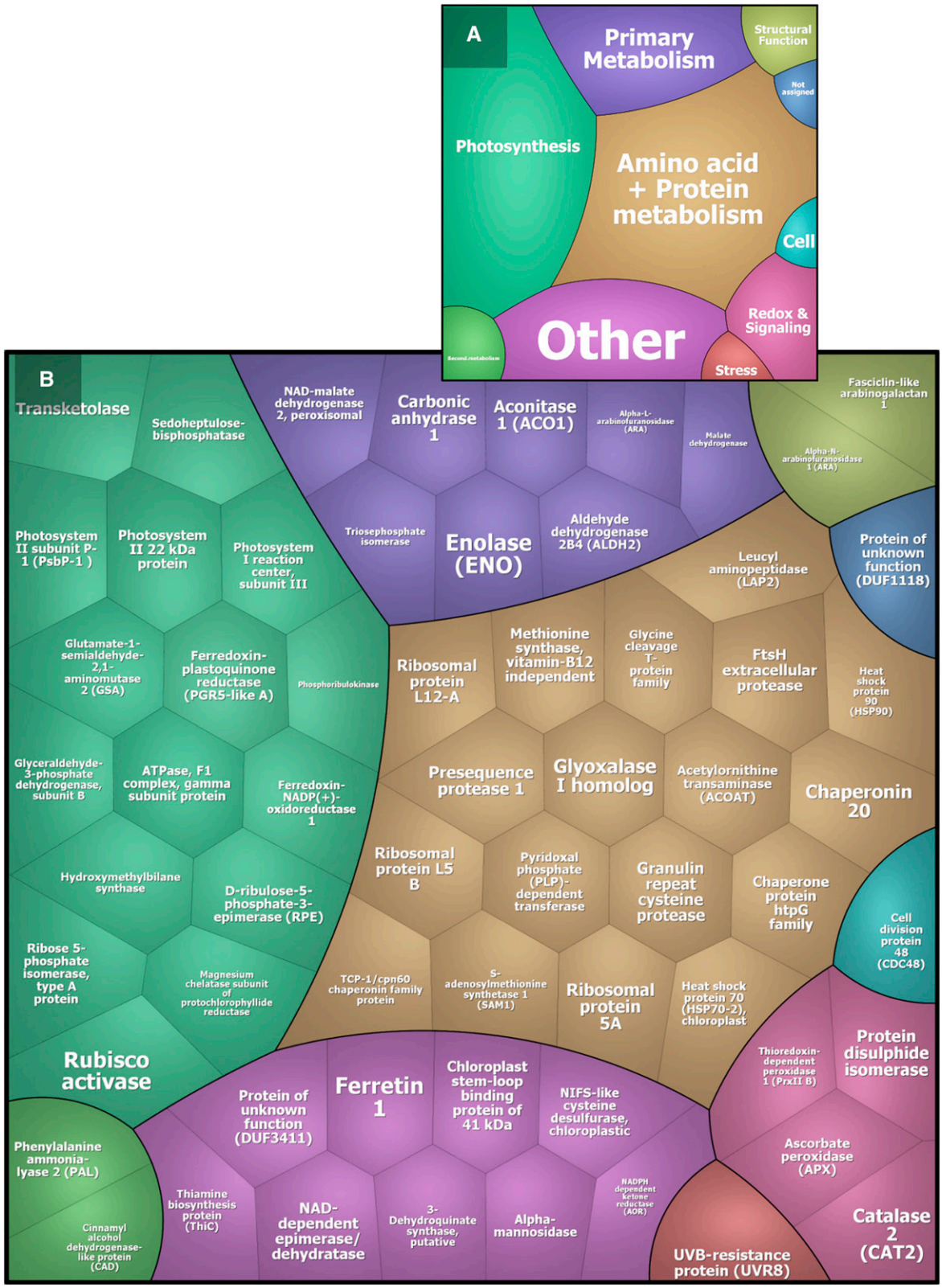

Figure 4. Voronoi Treemaps showing the 63 *S*-nitrosylated proteins discriminant in IE and NE genotypes (Supplemental Table S4) and assigned to functional categories at the first level (A) and the third level (B).

interferes in the signaling pathway activated by NO-ROS interactions.

Comparison of the IE and NE S-Nitroso-Proteome Reveals the Consequences of Isoprene Suppression in Poplar Plants following Acute Ozone

Irrespective to the plant genotypes, ozone induced strong changes in the *S*-nitroso-proteome. Possible changes in global protein abundance by the ozone treatment have been taken into account. The intensities of the *S*-nitrosylated proteins were normalized to the corresponding global protein abundances of the control and ozone-treated leaves.

Principal component analysis (PCA) with these normalized data revealed that the pronounced differences in the abundance of *S*-nitrosylated proteins between NE and IE genotypes appear after ozone treatment, as indicated by a clear separation between ozonated NE and IE samples in the first and second principal components (Supplemental Fig. S1A). The functional categorization of the 203 *S*-nitrosylated proteins revealed a strong dominance of proteins related to photosynthetic processes (21%), followed by protein synthesis, degradation and folding processes (19%), and redox regulation and signaling (8%; Supplemental Fig. S1B; Supplemental Table S2).

We again used the OPLS method to study the *S*-nitroso-protein patterns of control and ozonated samples in more detail (Fig. 5). The separation between treatments and genotypes can be explained by the 63 discriminant *S*-nitrosylated proteins (out of 203; Fig. 4; Supplemental Table S4).

The general ozone response shared by both genotypes demonstrated a strong ozone-induced increase in the abundance of *S*-nitrosylated proteins, but the changes in the *S*-nitroso-proteome of the NE genotype were much more pronounced than in the IE genotype. While in IE plants, the *S*-nitrosylation level of 16 proteins (13 up and three down) was changed upon acute ozone stress (Fig. 6C; Supplemental Table S5A), the *S*-nitrosylation level of 54 proteins (53 up and one down) was altered in the NE genotype upon ozone treatment (Fig. 6E; Supplemental Table S5B).

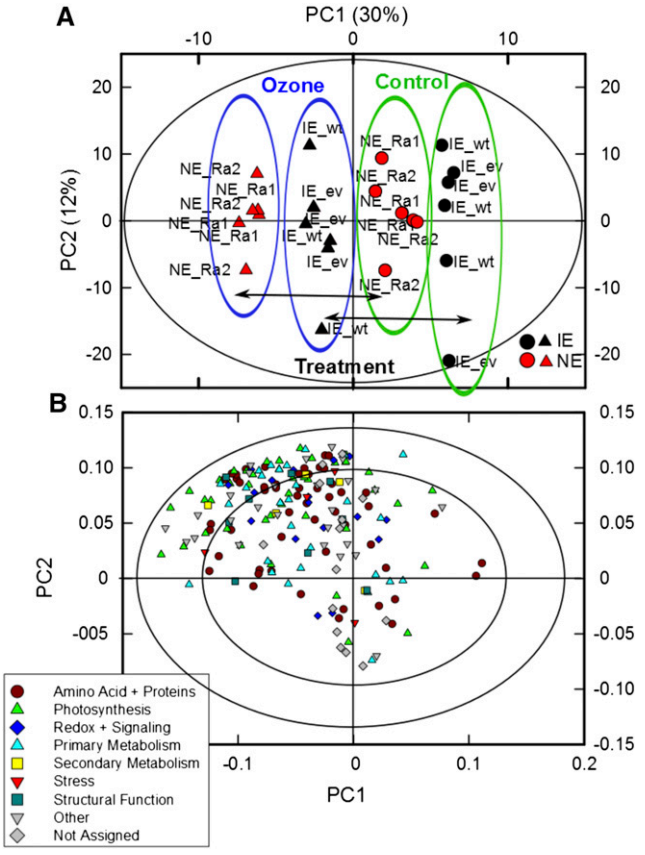

Figure 5. Score (A) and loading (B) plots of the OPLS of *S*-nitrosylated protein abundances from control and ozone samples of IE (wild type [wt] and EV) and NE (Ra1 and Ra2) genotypes. A, Plants were divided into the ozone group (triangles; $n = 12$) and the control group (circles; $n = 12$). The ellipse indicates the tolerance based on Hotelling's t^2 with a significance level of 0.05. B, Each functional group of proteins is indicated with different colors. The outer and inner ellipses indicate 100% and 75% explained variance, respectively. Each point represents an independent plant in the score plot and an individual protein in the loading plot. OPLS model fitness is as follows: r^2 (x) = 48.7%, r^2 (y) = 100%, r^2 = 69%, and q^2 (cumulative) = 59% using one predictive component. RMSEE (root mean square error of estimation) = 0.224 and RMSEcv (root mean square error of cross validation) = 0.293. P values of cross-validated ANOVA are as follows: NE/IE genotype, $P < 0.05$; ozone/control treatment, $P < 0.01$. PC, Principal component.

Target Sites of NO Action in IE and NE Gray Poplar

The *S*-nitroso-proteins, of which the *S*-nitrosylation abundances differ significantly between the IE and NE genotypes within the ozone-treated plants, are listed in Table I. These proteins belong to several pathways, such as photosynthesis, the CBB cycle, glycolysis, the tricarboxylic acid cycle, redox metabolism, cell wall metabolism, amino acid degradation, and metal handling (Fig. 6F).

Carbon Metabolism and Photosynthetic Proteins in the NE Genotype. Many enzymes and structural components of carbon metabolism, and thus of photosynthesis and catabolizing pathways (glycolysis and the tricarboxylic acid cycle), became *S*-nitrosylated upon ozone treatment (Fig. 5; Supplemental Tables S3 and S4), and for most of the enzymes, the ozone treatment modulated the *S*-nitrosylation pattern of IE and NE genotypes differentially (Table I; Fig. 6F). Notably, many enzymes of the CBB cycle became more *S*-nitrosylated in the NE genotype compared with the IE genotype when acutely stressed by ozone. These enzymes are sedoheptulose bisphosphatase (SBPase), Rubisco activase, ribose-5-phosphate isomerase, PRK, glyceraldehyde-3-phosphate dehydrogenase (GAPDH), triosephosphate isomerase (TPI), and phosphoglycerate kinase. SBPase and TPI became *S*-nitrosylated in NE plants upon ozone treatment, whereas the corresponding amount of protein was

Figure 6. A and B, Voronoi Treemaps showing changes in the *S*-nitroso-proteome depending on ozone or control (O/C) treatment (A) and NE or IE genotype (B). C and E, Ozone-induced changes in the *S*-nitroso-proteome of IE (wild type and EV; C) and NE (Ra1 and Ra2; E) genotypes. D and F, Ratios of *S*-nitrosylation rates in NE/IE genotypes under control conditions (D) and ozone treatment (F). *S*-Nitrosylated proteins were assigned to the functional categories displayed in Figure 4. Expression changes ($\log_2$ ratios of two conditions) were color coded: orange indicates increased ($\log_2$ ratio −3), gray indicates unchanged, and blue indicates decreased ($\log_2$ ratio 3) expression.

constitutively down-regulated in NE control plants, emphasizing that many proteins are regulated on several levels. Out of the group of CBB cycle enzymes, only TPI and Rubisco have been biochemically characterized, and both appeared to be inhibited by *S*-nitrosylation (Abat et al., 2008; Abat and Deswal, 2009; Zaffagnini et al., 2014). The cytosolic GAPDH was reported to be inhibited by *S*-nitrosylation as well (Holtgrefe et al., 2008; Zaffagnini et al., 2013). However, it is unclear if this is true for the chloroplastic GAPDH, which shares only low structural similarity with the cytosolic isoenzyme (Shih et al., 1991). In Arabidopsis (*Arabidopsis thaliana*) *S*-nitrosoglutathione reductase knockout plants, the *S*-nitrosylated proteins are enriched significantly in chlorophyll metabolism and photosynthesis. These plants consistently show lower chlorophyll levels and altered photosynthetic properties, suggesting that *S*-nitrosylation is an important regulatory mechanism in these processes (Hu et al., 2015).

The tricarboxylic acid cycle enzymes malate dehydrogenase and ACONITASE1 (ACO1) showed increases of the *S*-nitrosylation level upon ozone exposure in the NE genotype (Table I; Fig. 6F). Both enzymes become inactivated by *S*-nitrosylation (Gupta et al., 2012; Ortega-Galisteo et al., 2012). Inactivation of ACO1 by NO leads to an accumulation of citrate, which, as a retrograde signal, induces alternative oxidase, resulting in a stimulation of nitrogen and amino acid metabolism (Gupta et al., 2012). The comprehensive metabolomic analyses of the NE and IE genotypes (Way et al., 2013; Kaling et al., 2015) revealed increased concentrations of compounds from amino acid metabolism, the tricarboxylic acid cycle, and glycolysis. These findings suggest that the tricarboxylic acid cycle and perhaps glycolysis are constitutively down-regulated in NE plants compared with IE plants and become even more repressed during oxidative/nitrosative stress.

Table I. *Log fold changes of the abundances of S-nitrosylated proteins between IE and NE gray poplar after ozone fumigation (only ozone samples) that differ significantly between lines (variable of importance for the projection [VIP] score)*

The intensities of the *S*-nitrosylated proteins were normalized to the corresponding global protein abundances of ozone-treated leaves. Functional categorization was done according to MapMan BIN (http://ppdb.tc.cornell.edu/dbsearch/searchacc.aspx). Asterisks indicate LC-MS/MS quantification based on one unique peptide. Dashes indicate SE values > VIP score.

Accession	VIP Score	SE	Log_2 NE/IE	Annotation	MapMan BIN Category	*P* (Student's *t* Test)
POPTR_0004s01030	1.73	0.60	0.9	Gly cleavage T-protein family	Amino acid metabolism/degradation	0.091
POPTR_0004s01320*	1.49	0.78	0.7	Glyoxalase I homolog	Amino acid metabolism/degradation	0.075
POPTR_0001s37650*	1.61	0.58	0.5	Fasciclin-like arabinogalactan1	Cell wall	0.115
POPTR_0016s02620*	1.36	1.07	0.8	α-*N*-Arabinofuranosidase1 (ARA1)	Cell wall	0.023
POPTR_0006s02850*	<1	–	0.6	α-*N*-Arabinofuranosidase (ARA)	Cell wall	0.045
POPTR_0006s12740*	1.45	1.08	1.6	Cell division protein48 (CDC48)	Cell division	0.065
POPTR_0001s25630*	1.92	0.74	1.0	Thiamine biosynthesis protein (ThiC)	Cofactor and vitamin metabolism	0.025
POPTR_0015s08540*	2.08	0.66	1.5	Aldehyde dehydrogenase2B4	Fermentation	0.010
POPTR_0008s05640	1.61	0.46	1.0	Triosephosphate isomerase (TPI)	Glycolysis	0.007
POPTR_0008s08400*	<1	–	1.1	Phosphoglycerate kinase	Glycolysis	0.013
POPTR_0006s10480	1.50	0.86	0.9	Ferretin1	Metal handling	0.079
POPTR_0016s14950*	<1	–	1.6	2,3-Bisphosphoglycerate mutase, putative	Metal handling/binding, chelation, and storage	0.002
POPTR_0016s14310	1.54	0.74	0.4	NADPH-dependent ketone reductase (AOR)	Miscellaneous	0.052
POPTR_0006s19810*	1.48	0.83	1.0	Leucyl aminopeptidase (LAP2)	Protein degradation	0.008
POPTR_0001s35230*	1.73	0.83	1.4	Ribosomal protein L12-A	Protein synthesis	0.008
POPTR_0001s26970*	<1	–	1.6	Ribosomal protein	Protein synthesis	0.009
POPTR_0004s23490*	<1	–	1.7	Elongation factor 1 γ1, putative	Protein synthesis	0.024
POPTR_0002s00840	2.39	1.06	0.9	Glyceraldehyde-3-phosphate dehydrogenase, subunit B	Photosynthesis/Calvin cycle	0.135
POPTR_0010s20060	2.28	0.29	1.2	Sedoheptulose-1,7-bisphosphatase	Photosynthesis/Calvin cycle	0.000
POPTR_0010s20810	2.15	0.91	0.6	Rubisco activase	Photosynthesis/Calvin cycle	0.134
POPTR_0013s03700	1.79	0.59	0.5	Ribose 5-phosphate isomerase, type A protein	Photosynthesis/Calvin cycle	0.079
POPTR_0003s09830	1.63	0.84	0.6	Phosphoribulokinase (PRK)	Photosynthesis/Calvin cycle	0.009
POPTR_0001s08420*	1.55	0.94	0.9	Ferredoxin-plastoquinone reductase (PGR5-like A)	Photosynthesis/light reaction	0.001
POPTR_0008s15100*	1.14	0.48	3.1	PSI subunit D-2	Photosynthesis/light reaction	0.148
POPTR_0002s01080	1.55	0.80	0.8	Catalase2 (CAT2)	Redox	0.053
POPTR_0005s17350*	1.27	1.10	1.3	Ascorbate peroxidase (APX)	Redox	0.001
POPTR_0001s44990*	1.18	1.00	1.0	Thioredoxin-dependent peroxidase1 (PrxII B)	Redox	0.011
POPTR_0009s02070	<1	–	0.7	Ascorbate peroxidase (APX)	Redox	0.020
POPTR_0009s07040*	2.33	0.83	0.7	NIFS-like Cys desulfurase, chloroplastic	*S* assimilation	0.131
POPTR_0002s01990*	1.82	0.53	1.2	Cinnamyl alcohol dehydrogenase-like protein (CAD)	Secondary metabolism	0.011
POPTR_0007s04700*	1.89	1.18	1.7	UV-B resistance protein (UVR8)	Stress/abiotic	0.043
POPTR_0005s10990	2.03	1.24	0.6	Aconitase1 (ACO1)	Tricarboxylic acid/organ transformation	0.064
POPTR_0008s16670	1.36	1.08	1.2	Malate dehydrogenase	Tricarboxylic acid/organ transformation	0.002

Antioxidant Enzymes in the NE Genotype. Several antioxidant enzymes (i.e. CATALASE2, APX, THIOREDOXIN-DEPENDENT PEROXIDASE1) also showed more pronounced *S*-nitrosylation levels in the NE genotype compared with the IE genotype (Table I; Fig. 6F). Transgenic plants with reduced protein levels or activities of CAT and APX revealed accumulations of H_2O_2, an early event in PCD (Dat et al., 2003), and cytosolic APX was found to be *S*-nitrosylated at the onset of PCD (de Pinto et al., 2013; Lindermayr and Durner, 2015; Yang et al., 2015). The enhanced *S*-nitrosylation of CAT and APX in the NE genotype upon ozone fumigation may analogically lead to increased H_2O_2 levels compared with the IE genotype. Interestingly, chloroplast (Velikova et al., 2014) and whole-proteome (Supplemental Table S1) analyses reveal that the protein levels of several antioxidant enzymes are constitutively lower in the NE genotype (e.g. APX, SOD, and chloroplastic peroxiredoxin). By contrast, total ascorbate content was found to be higher in NE plants (Behnke et al., 2009; Way et al., 2013) compared with IE plants. Ascorbate can scavenge ROS directly or act as a reducing substrate for APX (Foyer and Noctor, 2011). It was suggested earlier that the increase of nonvolatile antioxidant metabolites in the NE genotype might compensate for

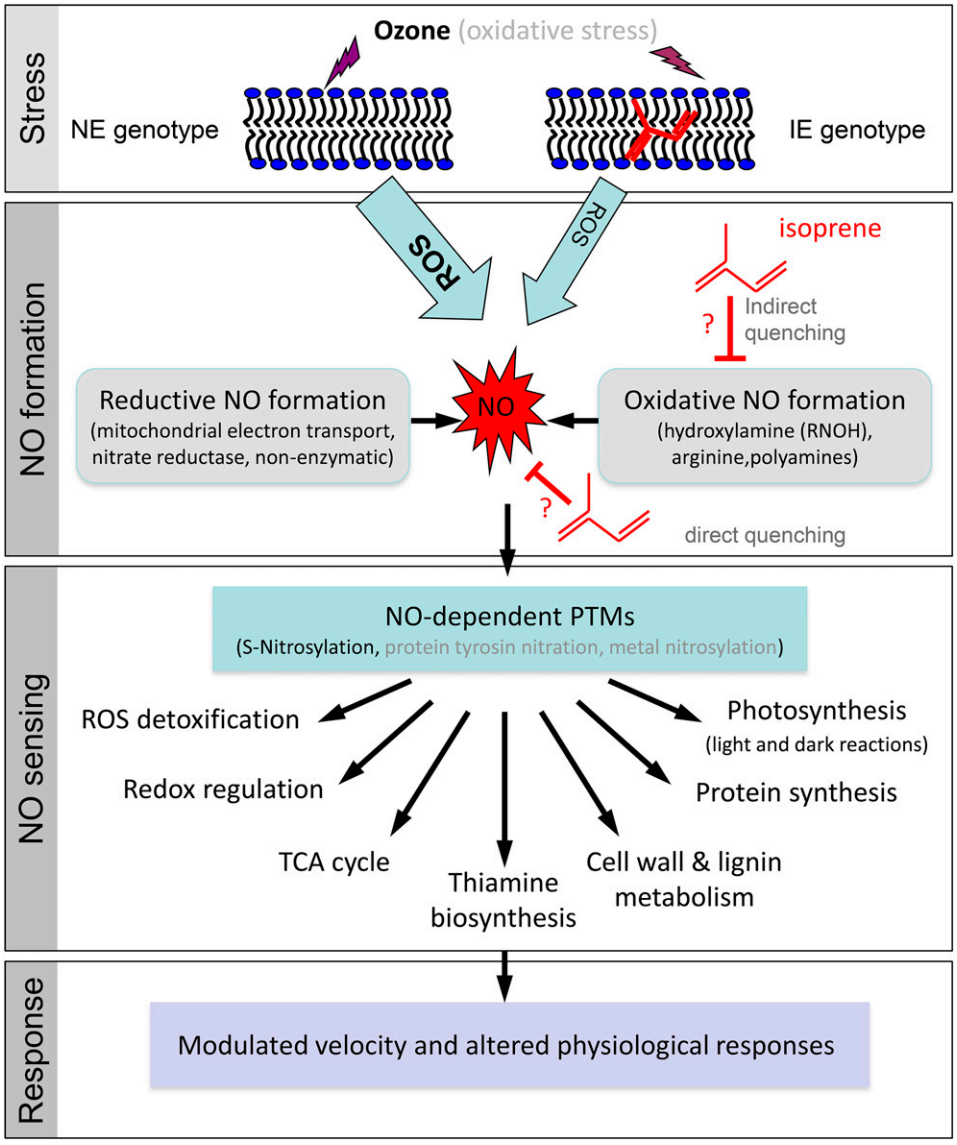

Figure 7. Scheme of the possible interactions of isoprene with NO formation processes and biochemical target sites of NO in NE gray poplar (modified from Moreau et al., 2010). TCA, Tricarboxylic acid.

the absence of isoprene (Behnke et al., 2009; Way et al., 2013). In view of our data here, we assume that the altered *S*-nitrosylation status of many ROS-metabolizing enzymes results in a higher oxidative load in plant cells where isoprene is absent. This difference in the cellular redox homeostasis of both genotypes likely exists under physiological (unstressed) conditions, as indicated by higher H_2O_2 levels in the light-exposed chloroplasts of NE leaves (Behnke et al., 2010a).

Cell Wall- and Lignin Biosynthesis-Related Proteins in the NE Genotype. The *S*-nitrosylation levels of proteins involved in cell wall reconstruction and lignin biosynthesis also were increased by ozone stress in the NE genotype compared with the IE genotype (Table I; Fig. 6F). These proteins are the two α-L-arabinofuranosidases proteins (ARA and the fasciclin-like arabinogalactan protein FLA) and the cinnamyl alcohol dehydrogenase-like protein CAD. FLAs are an expanded protein family in plants (Johnson et al., 2003) implicated in processes such as xylem differentiation, cell division, adhesion, and signaling (Janz et al., 2010; Seifert and Blaukopf, 2010). ARA, a glycosyl hydrolase, also is connected with secondary cell wall formation and cell wall reorganization (Sumiyoshi et al., 2013). Generally, poplar leaves respond to ozone stress with an up-regulation of gene expression and enzyme activities of phenylpropanoid and lignin biosynthetic proteins (Richet et al., 2012), which lead to higher contents of condensed lignin, hydroxycinnamic acids, and flavonoids (Booker and Miller, 1998; Cabané et al., 2004). We recently described the denitrosylation of PAL and COMT in wild-type gray poplar upon ozone exposure (Vanzo et al., 2014) and demonstrated for PAL that in vitro PAL activity increased as a result of denitrosylation.

Because PAL is a key regulatory enzyme controlling the metabolic flux in the phenylpropanoid and downstream biosynthetic pathways (Booker and Miller, 1998; Cabané et al., 2004), the activities of the other enzymes of the phenolic secondary metabolism, such as COMT (Vanzo et al., 2014) and CAD, also may be rapidly regulated by *S*-nitrosylation. In the NE genotype but not the IE genotype, the CAD protein, catalyzing the final step in the synthesis of monolignols (Di Baccio et al., 2008), was found to be *S*-nitrosylated after ozone exposure (Table I). However, whether these differences in *S*-nitrosylation levels are related to the constitutive and stress-induced metabolomic differences (Way et al., 2013; Kaling et al., 2015; i.e. of phenolic compounds in NE and IE genotypes) requires additional analysis.

Thiamine Biosynthetic Proteins in the NE Genotype. Interestingly, two enzymes of the thiamine biosynthetic pathway were identified as putative targets of *S*-nitrosylation (Fig. 4; Supplemental Table S2). These enzymes are the thiamine thiazole synthase and the thiamine biosynthesis protein, the latter showing an increase in *S*-nitrosylation in the NE genotype upon ozone treatment. Nontargeted metabolomics indicated that NE leaves have high levels of thiamine monophosphate (Way et al., 2013), a precursor of thiamine biosynthesis. Thiamine pyrophosphate is an important coenzyme required for many cellular processes, such as the tricarboxylic acid cycle and the methylerythritol phosphate pathway (Goyer, 2010), where it acts as a cofactor of 1-deoxy-D-xylulose-5-phosphate synthase (DXS). Chloroplasts of the NE genotype accumulate excessive amounts of dimethylallyl diphosphate, the metabolic precursor of isoprene (Ghirardo et al., 2014). Dimethylallyl diphosphate inhibits in vivo the activity of DXS (Ghirardo et al., 2014) by competing for the same substrate-binding site with thiamine pyrophosphate (Banerjee et al., 2013). Whether the differences in stress-induced changes in the *S*-nitrosylation of thiamine biosynthetic enzymes in NE and IE genotypes are regulatorily orchestrated with the differences of the tricarboxylic acid and methylerythritol phosphate pathway intermediates and PTMs, however, is unknown.

UV-B Photoreceptor in the NE Genotype. Ozone treatment led to a strong increase in the *S*-nitrosylation levels of the UV RESISTANCE LOCUS8 (UVR8) protein in both genotypes (Table I; Fig. 6A), with more pronounced *S*-nitrosylation in the NE genotype (Fig. 6E; Supplemental Table S5B). UVR8 is a receptor protein for UV-B radiation and localized as a homodimer in the cytosol (Rizzini et al., 2011). UV-B light induces dimer dissociation, the translocation of UVR8 monomers into the nucleus, and the activation of the transcription factors ELONGATED HYPOCOTYL5 and MYB12, leading to the expression of a range of genes encoding flavonoid biosynthetic enzymes, DNA repair machineries, and antioxidant proteins (Favory et al., 2009; Heijde and Ulm, 2012). It has been proposed that NO-mediated *S*-nitrosylation is involved in the nuclear translocation of UVR8 (Tossi et al., 2011), similar to the nuclear translocation of GAPDH undergoing *S*-nitrosylation (Hara et al., 2005). Our data here confirm UVR8 as a target of protein *S*-nitrosylation (Fig. 4; Supplemental Table S2). UV-B light exposure and ozone fumigation share many common metabolic and regulatory components, such as an increase in ROS formation and the upregulation of antioxidants (Rao et al., 1996). One may suggest that the *S*-nitrosylation of the UVR8 photoreceptor, triggering transcriptional changes favoring the production of ROS-quenching polyphenols (Quideau et al., 2011), may be a general response to oxidative stress. This assumption would indicate a higher amount of phenolic compounds in the NE genotype undergoing oxidative stress. However, UV-B light treatment of the NE genotype resulted in a reduced accumulation of UV-B light-absorbing compounds compared with the IE genotype (Kaling et al., 2015). Therefore, additional work is necessary to clarify the importance of UVR8 in the regulation of different regulations of phenolic compound accumulation in the NE genotype compared with the natural situation of isoprene emitters.

CONCLUSION

Our data demonstrate that the isoprene in poplar leaves influences rapid stress-induced changes in NO emission and thus in the pattern of the in vivo *S*-nitroso-proteome. In accordance with the higher NO emission rates in the NE genotype, the *S*-nitroso-proteome of this genotype was more susceptible to ozone-induced changes compared with IE plants. Our results demonstrate that the nitrosative pressure is lower when isoprene is present in leaf cells. The main target sites of NO action in NE poplar are proteins related to the light and dark reactions of photosynthesis, the tricarboxylic acid cycle, protein metabolism, and redox regulation (Fig. 7). CAT2, APX, and THIOREDOXIN-DEPENDENT PEROXIDASE1, all being involved in the detoxification of ROS (Mittler, 2002), showed increases in *S*-nitrosylation in NE plants upon oxidative stress. These results indicate that isoprene indirectly regulates ROS formation via the control of the *S*-nitrosylation levels of ROS-metabolizing enzymes. There is evidence (Ortega-Galisteo et al., 2012; de Pinto et al., 2013) that *S*-nitrosylation inhibits the activities of CAT and APX, thus increasing the accumulation of H_2O_2 (Dat et al., 2003; Vandenabeele et al., 2004; Davletova et al., 2005) as a prerequisite of the plant's defense response (Apel and Hirt, 2004; de Pinto et al., 2006). Considering the observed lower constitutive amount of many antioxidative enzymes in the NE proteome, our data indicate that the antioxidative defense system in poplar that maintains ROS production under strict control is rearranged in the NE genotype at the protein level and at the level of protein *S*-nitrosylation.

Overall, the data strongly support the hypothesis (Vickers et al., 2009a) that unsaturated volatile isoprenoids such as isoprene can alter signaling pathways by modulating to what extent and how rapidly ROS and NO signaling molecules are generated within a cell, thus likely modulating the velocity and extent of the physiological response upon biotic and abiotic stress (Ahlfors et al., 2009; Wang et al., 2013).

MATERIALS AND METHODS

Plant Material and Growth Conditions

All experiments were performed with the natural hybrid (wild-type) gray poplar (*Populus* × *canescens*; Institut National de la Recherche Agronomique clone 7171-B4; syn. *Populus tremula* × *Populus alba*), a naturally strong isoprene emitter. Additionally, EV control plants were used. In addition to these two IE lines, two well-characterized NE lines (35S::*PcISPS* RNA interference lines Ra1 and Ra2; Behnke et al., 2007) were chosen for the experiments. Plantlets were amplified by micropropagation and cultivated (27°C/24°C day/night, 16-h photoperiod, and approximately 100 μmol photons m^{-2} s^{-1}) under sterile conditions on one-half-concentrated Murashige and Skoog medium in 1-L glass containers each accommodating six to seven plantlets. Every 8 to 10 weeks, plantlets were transferred to fresh medium. Rooting shoots were transferred to soil substrate (50% [v/v] Fruhstorfer Einheitserde and 50% [v/v] silica sand [particle size, 1–3 mm]) and grown under a plastic lid to maintain high humidity. Plantlets were adapted to ambient air by gradually opening the lid. After approximately 4 weeks on soil, plants were transferred to bigger pots (2.2 L; 25% [v/v] Fruhstorfer Einheitserde, 25% [v/v] silica sand, and 50% [v/v] perlite) and further cultivated in the greenhouse. The soil was initially mixed with a slow-release fertilizer (Triabon [Compo] and Osmocote [Scotts Miracle-Gro]; 1:1, 10 g L^{-1} soil). Climate conditions in the greenhouse were as follows: 22°C/18°C day/night, 16-h photoperiod, and supplemental lighting was used (200–240 μmol photons m^{-2} s^{-1}).

Experimental Setup and Ozone Fumigation

The ozone experiment was performed in two sun simulators (for details, see Thiel et al., 1996) in Munich, Germany. The sun simulators mimic the spectral irradiance in nature nearly perfectly, simulating natural irradiation. In both chambers (control and ozone), 24 8-week-old plants were placed (six plants from each genotype; IE: wild type and EV; NE: Ra1 and Ra2) and acclimated to the prevailing temperature and light conditions (27°C/18°C day/night and approximately 800 μmol photons m^{-2} s^{-1}) for 7 d. The ozone pulse (800 nL L^{-1} for 1 h) was given at 10 AM. Immediately after fumigation, leaves 9 and 10 (counted from the apex) were frozen in liquid nitrogen for later biochemical and proteomic analyses.

Analysis of NO Emissions following Acute Ozone Exposure

Measurements were made at the branch level in a dynamic cuvette system (Vanzo et al., 2014). Whole plants were cut and immediately recut under water, and a branch with 18 leaves was introduced into a gas-tight glass cuvette (38.3 L, 500 μmol m^{-2} s^{-1} photosynthetic photon flux density, air temperature 25°C ± 1°C, and flux 11.5 L min^{-1}) and exposed to synthetic air made by mixing pure oxygen, N_2, and CO_2 from cylinders. Concentrations of the three gases (20%, 80%, and 400 μL L^{-1}, respectively) were set with mass-flow controllers. Net CO_2 assimilation and transpiration were monitored as differences between cuvette inlet and outlet air by infrared absorption (Fischer-Rosemount Binos 100 4P). When net CO_2 assimilation was stable, ozone fumigation (with 800 nL L^{-1}) was applied for 1 h. Part of the cuvette outflow was diverted to an NO-NO_2-NO_3 analyzer (Eco Physics; model CLD 88 Y p). The detection limit of this instrument is 50 pL L^{-1}. NO emission (Φ_{NO}; nmol mol^{-1}) from the leaves was calculated as described by Velikova et al. (2008). Calculations were made based on the gas diffusion: $\Phi_{NO} = [NO_{cv} \times \Phi_{air}]/S$, where NO_{cv} (nmol mol^{-1}) is the NO concentration in the cuvette, Φ_{air} (mol s^{-1}) is the air flow rate in the cuvette, and S (m^2) is the leaf area in the cuvette.

Biotin-Switch Assay and LC-MS/MS-Based Identification and Quantification of *S*-Nitrosylated Proteins

Six biological replicates per treatment were analyzed from each genotype (IE: wild type and EV; NE: Ra1 and Ra2). The detection of in vivo *S*-nitrosylated proteins was performed via a modified biotin-switch assay (Vanzo et al., 2014). Frozen leaf powder was mixed with HENT buffer (100 mM HEPES-NaOH, pH 7.4, 10 mM EDTA, 0.1 mM Neocuproine, and 1% [v/v] Triton X-100) in a mixing ratio of leaf powder:buffer 1:5 (w/v). The HENT buffer contained 30 mM *N*-ethylmaleimide (NEM) and protease inhibitor cocktail tablets (Complete; Roche). The homogenate was mixed on a shaker for 30 s, incubated on ice for 15 min, and centrifuged twice (14,000*g* for 10 min). The protein concentration of the supernatant was adjusted to 1 μg μL^{-1} with HENT buffer. For blocking, 4 times the volume (v/v) of HENS (225 mM HEPES-NaOH, pH 7.2, 0.9 mM EDTA, 0.1 mM Neocuproine, and 2.5% [w/v] SDS) was freshly prepared, and 30 mM NEM was added to the protein extracts. The samples were incubated at 37°C for 30 min. Excess NEM was removed by precipitation with ice-cold acetone, and the protein pellets were resuspended in 0.5 mL of HENS buffer (without NEM) per mg of protein in the starting sample. Biotinylation was achieved by adding pyridyldithiol-biotin and sinapic acid (1 and 3 mM final concentrations, respectively) with further dark incubation at room temperature for 1 h. The controls for false-positive signals were treated with SIN in the presence of NEM for 25 min at 37°C before the biotinylation step (Supplemental Fig. S2). After biotinylation, the proteins were precipitated with acetone and subjected to affinity purification of biotinylated proteins by NeutrAvidin agarose, as described elsewhere (Lindermayr et al., 2005). For affinity purification of biotinylated proteins, the precipitated proteins were resuspended in HENS buffer (100 μL mg^{-1} protein in the starting sample) and 2 volumes of neutralization buffer (20 mM HEPES, pH 7.7, 100 mM NaCl, 1 mM EDTA, and 0.5% [v/v] Triton X-100). Biotinylated proteins were incubated for 1 h at room temperature with the NeutrAvidin agarose (30 μL mg^{-1} protein). The agarose matrix was washed extensively with 20 volumes of washing buffer (600 mM NaCl in neutralization buffer), and bound proteins were eluted with 100 mM β-mercaptoethanol in elution buffer (20 mM HEPES, pH 7.7, 100 mM NaCl, and 1 mM EDTA) and precipitated with ice-cold acetone.

In-Solution Digestion of *S*-Nitrosylated Proteins after NeutrAvidin Affinity Purification

The pellets from the acetone precipitation were dissolved in 30 μL of 50 mM ammonium bicarbonate. For protein reduction, 2 μL of 100 mM dithiothreitol was added and incubated for 15 min at 60°C. After cooling to room temperature, the free Cys residues were alkylated by adding 2 μL of freshly prepared 300 mM iodoacetamide solution for 30 min. A tryptic digestion was performed overnight at 37°C using 0.5 μg of trypsin (Promega) per sample. The digestion was stopped by adding trifluoroacetic acid and then stored at −20°C.

Preparation of Whole-Cell Extracts for Overall Proteomic Analyses

From each genotype (IE: wild type and EV; NE: Ra1 and Ra2), six biological replicates per treatment were analyzed. Fifty milligrams of frozen, homogenized leaf tissue was mixed with 1 mL of HENT buffer containing a protease inhibitor cocktail tablet and incubated on ice for 10 min. After centrifugation (14,000*g* for 10 min), Triton X-100 was removed by passing samples over a Sephadex G-25 column (GE Healthcare) using HEN buffer (without Triton X-100). After determination of the protein content by the Bradford assay, aliquots containing 10 μg of protein were prepared for LC-MS/MS analysis and subsequent label-free quantification.

Filter-Aided Proteome Preparation Digestion of Proteins from Whole-Cell Extracts

From each of the whole-cell extracts, an aliquot containing 10 μg of protein was digested using a modified filter-aided proteome preparation procedure (Wiśniewski et al., 2009). The proteins were reduced and alkylated using dithiothreitol and indole-3-acetic acid, centrifuged through a 30-kD cutoff filter device (PALL), and washed three times with UA buffer (8 M urea in 0.1 M Tris/HCl, pH 8.5) and twice with 50 mM ammonium bicarbonate. The proteins were digested for 2 h at room temperature using 1 μg of Lys-C (Wako Chemicals) and for 16 h at 37°C using 2 μg of trypsin (Promega). The peptides were collected by

centrifugation (10 min at 14,000*g*), and the samples were acidified with 0.5% trifluoroacetic acid and stored at −20°C.

Mass Spectrometry

Digested samples (after affinity purification or from whole-cell extracts) were thawed and centrifuged (14,000*g*) for 5 min at 4°C. LC-MS/MS analysis was performed as described previously on an Ultimate 3,000 nano-HPLC device coupled to an LTQ-OrbitrapXL (Thermo Fischer Scientific; Hauck et al., 2010). Every sample was automatically injected and loaded onto the trap column at a flow rate of 30 μL min^{-1} in 5% buffer B (98% acetonitrile/0.1% formic acid [v/v] in HPLC-grade water [v/v]) and 95% buffer A (2% acetonitrile/0.1% formic acid [v/v] in HPLC-grade water [v/v]). After 5 min, the peptides were eluted from the trap column and separated on the analytical column by a 135-min gradient from 7% to 32% acetonitrile in 0.1% formic acid at a flow rate of 300 nL min^{-1} followed by a short gradient from 32% to 93% acetonitrile for 5 min. The gradient was set back between each sample to starting conditions and left to equilibrate for 20 min. The 10 most abundant peptide ions from the mass spectrometry prescan were fragmented in the linear ion trap if they showed an intensity of at least 200 counts and if they were at least +2 charged. During fragmentation, a high-resolution (6×10^4 full-width half-maximum at 400 mass-to-charge ratio) mass spectrometry spectrum was acquired in the Orbitrap with a mass range from 300 to 1,500 D.

Label-Free Analysis Using Progenesis LC-MS Software

The acquired spectra were loaded onto the Progenesis LC-MS software (version 2.5; Nonlinear Dynamics) for label-free quantification and analyzed as described previously (Hauck et al., 2010; Merl et al., 2012). Features with only one charge or features with more than seven charges were excluded. The raw abundances of the remaining features were normalized to allow for the correction of factors resulting from experimental variation. Rank 1 to 3 tandem mass spectrometry spectra were exported as a MASCOT generic file and used for peptide identification with MASCOT (versions 2.2 and 2.3.02; Matrix Science) in the *Populus trichocarpa* protein database (version 4; 17,236,452 residues and 45,036 sequences). The search parameters were 10 μL L^{-1} peptide mass and 0.6 D tandem mass spectrometry tolerance, with one missed cleavage allowed.

For the identification and quantification of *S*-nitroso-proteins, *N*-ethylmaleinimidation and carbamidomethylation were set as variable modifications, as well as Met oxidation. A MASCOT-integrated decoy database search calculated a false discovery rate of 0.17% using a MASCOT ion score cutoff of 30 and a significance threshold of $P < 0.01$.

For the identification and quantification of total proteins in whole-cell extracts of leaves, carbamidomethylation was set as a fixed modification, and Met oxidation and deamination of Asn/Gln were set as variable modifications. A MASCOT-integrated decoy database search calculated a false discovery rate of less than 1%. The MASCOT Percolator algorithm was used to distinguish between correct and incorrect spectrum identifications (Brosch et al., 2009), with a maximum *q* value of 0.01. Peptides with a minimum Percolator score of 15 were used further.

For each data set, the peptide assignments were reimported into the Progenesis LC-MS software. After summing up the abundances of all the peptides that were allocated to each protein, the identification and quantification results were exported and are given in Supplemental Table S6.

Visualization of Proteome Data

For proteomics visualization, we applied Voronoi Treemaps as introduced by Bernhardt et al. (2009). The presented Treemaps subdivide the two-dimensional plane into subsections according to the hierarchical data structure of gene functional assignments as taken from the corresponding Arabidopsis (*Arabidopsis thaliana*) orthologs (http://www.arabidopsis.org/tools/bulk/go/index.jsp), which were obtained via the POPGENIE (http://www.popgenie.org) database. For the top level, the total area is subdivided into main categories, then the main categories into subcategories and the subcategories into equally sized cells representing significantly changed proteins. According to this classification, HSP70 (Fig. 2B) was assigned to the subcategory protein folding (Fig. 2A) and this to the category amino acid and protein synthesis (Fig. 2A). In the overview images, functional classes were encoded using colors depending on categories. Expression change was encoded using a blue-to-gray-to-orange color gradient, with blue for decreased, gray for unchanged, and orange for increased expression.

Statistics

Differences in the overall proteome and the *S*-nitroso-proteome of the IE and NE genotypes between control and ozone-treated samples were analyzed as described previously (Vanzo et al., 2014) using PCA and OPLS statistical methods from the software package SIMCA-P (version 13.0.0.0; Umetrics). The results were validated by full cross validation (Erikssonet al., 2006) using a 95% confidence level.

Raw abundances from the label-free analysis of the proteome were extracted from the Progenesis LC-MS software (version 2.5; Nonlinear Dynamics). Protein intensities were normalized to the corresponding (averaged) protein abundance in whole-cell extracts of the control and ozone-treated leaves. PCA was performed on normalized, summed *S*-nitroso-protein intensities (centered and scaled with 1 SD^{-1}), which were preprocessed by logarithmic (base 10) transformation and used as x variables. Six independent biological replicates were used for each control and ozone treatment and for IE and NE genotypes, respectively. The size of the analyzed matrix was $2,024 \times 24$ and 206×24 for the overall proteome and the *S*-nitroso-proteome, respectively. The OPLS method was performed as PCA by giving as the y variable a value of 0 to control samples and a value of 1 to ozone samples. *S*-Nitroso-proteins showing a VIP value greater than 1 and uncertainty bars of the jack-knifing method less than the respective VIP value were defined as discriminant proteins that can separate ozone from control samples and IE from NE samples. Additionally, discriminant proteins were tested for significant differences ($P < 0.05$) between control and ozone samples using Student's t test and two-way ANOVA (SPSS version 22.0; SPSS).

Supplemental Data

The following supplemental materials are available.

Supplemental Figure S1. *S*-Nitrosylated proteins detected in the control and ozone samples of the IE and NE genotypes.

Supplemental Figure S2. Detection of endogenously *S*-nitrosylated proteins in NE gray poplar.

Supplemental Table S1. Proteins that discriminantly separate NE from IE gray poplar samples in the OPLS model of the whole proteome.

Supplemental Table S2. Complete list of LC-MS/MS-identified *S*-nitrosylated proteins in IE and NE gray poplar leaves (control and ozone).

Supplemental Table S3. Constitutively *S*-nitrosylated proteins that are differentially abundant in IE and NE gray poplar under steady-state conditions (only control samples).

Supplemental Table S4. Proteins that discriminantly separate NE from IE gray poplar samples in the control and ozone treatments in the OPLS model of the *S*-nitroso-proteome.

Supplemental Table S5. *S*-Nitrosylated proteins that are differentially abundant in ozone and control treatments of IE and NE gray poplar samples.

Supplemental Table S6. Full data set for the identification of total proteins from whole-cell extracts and *S*-nitroso-proteins with corresponding protein abundances after label-free quantification.

ACKNOWLEDGMENTS

We thank Andreas Albert and Hans Lang for helping with the sun simulator experiment, the ozone fumigation, and NO analysis as well as Ina Zimmer for technical laboratory assistance.

Received November 25, 2015; accepted February 4, 2016; published February 5, 2016.

LITERATURE CITED

Abat JK, Deswal R (2009) Differential modulation of S-nitrosoproteome of *Brassica juncea* by low temperature: change in S-nitrosylation of Rubisco is responsible for the inactivation of its carboxylase activity. Proteomics **9:** 4368–4380

Abat JK, Mattoo AK, Deswal R (2008) S-Nitrosylated proteins of a medicinal CAM plant *Kalanchoe pinnata*: ribulose-1,5-bisphosphate carboxylase/oxygenase activity targeted for inhibition. FEBS J **275:** 2862–2872

Affek HP, Yakir D (2002) Protection by isoprene against singlet oxygen in leaves. Plant Physiol **129:** 269–277

Ahlfors R, Brosché M, Kollist H, Kangasjärvi J (2009) Nitric oxide modulates ozone-induced cell death, hormone biosynthesis and gene expression in *Arabidopsis thaliana*. Plant J **58:** 1–12

Alvarez C, Lozano-Juste J, Romero LC, García I, Gotor C, León J (2011) Inhibition of Arabidopsis O-acetylserine(thiol)lyase A1 by tyrosine nitration. J Biol Chem **286:** 578–586

Apel K, Hirt H (2004) Reactive oxygen species: metabolism, oxidative stress, and signal transduction. Annu Rev Plant Biol **55:** 373–399

Aspeborg H, Schrader J, Coutinho PM, Stam M, Kallas A, Djerbi S, Nilsson P, Denman S, Amini B, Sterky F, et al (2005) Carbohydrate-active enzymes involved in the secondary cell wall biogenesis in hybrid aspen. Plant Physiol **137:** 983–997

Astier J, Kulik A, Koen E, Besson-Bard A, Bourque S, Jeandroz S, Lamotte O, Wendehenne D (2012) Protein S-nitrosylation: what's going on in plants? Free Radic Biol Med **53:** 1101–1110

Banerjee A, Wu Y, Banerjee R, Li Y, Yan H, Sharkey TD (2013) Feedback inhibition of deoxy-D-xylulose-5-phosphate synthase regulates the methylerythritol 4-phosphate pathway. J Biol Chem **288:** 16926–16936

Behnke K, Ehlting B, Teuber M, Bauerfeind M, Louis S, Hänsch R, Polle A, Bohlmann J, Schnitzler JP (2007) Transgenic, non-isoprene emitting poplars don't like it hot. Plant J **51:** 485–499

Behnke K, Kaiser A, Zimmer I, Brüggemann N, Janz D, Polle A, Hampp R, Hänsch R, Popko J, Schmitt-Kopplin P, et al (2010a) RNAi-mediated suppression of isoprene emission in poplar transiently impacts phenolic metabolism under high temperature and high light intensities: a transcriptomic and metabolomic analysis. Plant Mol Biol **74:** 61–75

Behnke K, Kleist E, Uerlings R, Wildt J, Rennenberg H, Schnitzler JP (2009) RNAi-mediated suppression of isoprene biosynthesis in hybrid poplar impacts ozone tolerance. Tree Physiol **29:** 725–736

Behnke K, Loivamäki M, Zimmer I, Rennenberg H, Schnitzler JP, Louis S (2010b) Isoprene emission protects photosynthesis in sunfleck exposed Grey poplar. Photosynth Res **104:** 5–17

Benhar M, Forrester MT, Stamler JS (2009) Protein denitrosylation: enzymatic mechanisms and cellular functions. Nat Rev Mol Cell Biol **10:** 721–732

Bernhardt J, Funke S, Hecker M, Siebourg J (2009) Visualizing gene expression data via Voronoi Treemaps. *In* Sixth International Symposium on Voronoi Diagrams, Copenhagen, Denmark, June 23-26, 2009, p. 233-241 IEEE Computer Society, Washington DC, USA, DOI: 10.1109/ISVD.2009.33.

Bethke PC, Gubler F, Jacobsen JV, Jones RL (2004) Dormancy of Arabidopsis seeds and barley grains can be broken by nitric oxide. Planta **219:** 847–855

Booker FL, Miller JE (1998) Phenylpropanoid metabolism and phenolic composition of soybean [*Glycine max* (L.) Merr.] leaves following exposure to ozone. J Exp Bot **49:** 1191–1202

Brosch M, Yu L, Hubbard T, Choudhary J (2009) Accurate and sensitive peptide identification with Mascot Percolator. J Proteome Res **8:** 3176–3181

Cabané M, Pireaux JC, Léger E, Weber E, Dizengremel P, Pollet B, Lapierre C (2004) Condensed lignins are synthesized in poplar leaves exposed to ozone. Plant Physiol **134:** 586–594

Cai B, Zhang A, Yang Z, Lu Q, Wen X, Lu C (2010) Characterization of photosystem II photochemistry in transgenic tobacco plants with lowered Rubisco activase content. J Plant Physiol **167:** 1457–1465

Corpas FJ, Chaki M, Leterrier M, Barroso JB (2009) Protein tyrosine nitration: a new challenge in plants. Plant Signal Behav **4:** 920–923

Corpas FJ, Leterrier M, Valderrama R, Airaki M, Chaki M, Palma JM, Barroso JB (2011) Nitric oxide imbalance provokes a nitrosative response in plants under abiotic stress. Plant Sci **181:** 604–611

Dat JF, Pellinen R, Beeckman T, Van De Cotte B, Langebartels C, Kangasjärvi J, Inzé D, Van Breusegem F (2003) Changes in hydrogen peroxide homeostasis trigger an active cell death process in tobacco. Plant J **33:** 621–632

Davletova S, Rizhsky L, Liang H, Shengqiang Z, Oliver DJ, Coutu J, Shulaev V, Schlauch K, Mittler R (2005) Cytosolic ascorbate peroxidase 1 is a central component of the reactive oxygen gene network of *Arabidopsis*. Plant Cell **17:** 268–281

Day CD, Lee E, Kobayashi J, Holappa LD, Albert H, Ow DW (2000) Transgene integration into the same chromosome location can produce alleles that express at a predictable level, or alleles that are differentially silenced. Genes Dev **14:** 2869–2880

Delledonne M, Xia Y, Dixon RA, Lamb C (1998) Nitric oxide functions as a signal in plant disease resistance. Nature **394:** 585–588

de Pinto MC, Locato V, Sgobba A, Romero-Puertas MdelC, Gadaleta C, Delledonne M, De Gara L (2013) S-Nitrosylation of ascorbate peroxidase is part of programmed cell death signaling in tobacco Bright Yellow-2 cells. Plant Physiol **163:** 1766–1775

de Pinto MC, Paradiso A, Leonetti P, De Gara L (2006) Hydrogen peroxide, nitric oxide and cytosolic ascorbate peroxidase at the crossroad between defence and cell death. Plant J **48:** 784–795

Di Baccio D, Castagna A, Paoletti E, Sebastiani L, Ranieri A (2008) Could the differences in O_3 sensitivity between two poplar clones be related to a difference in antioxidant defense and secondary metabolic response to O_3 influx? Tree Physiol **28:** 1761–1772

Durner J, Wendehenne D, Klessig DF (1998) Defense gene induction in tobacco by nitric oxide, cyclic GMP, and cyclic ADP-ribose. Proc Natl Acad Sci USA **95:** 10328–10333

Eriksson L, Johansson E, Kettaneh-Wold N, Trygg J, Wikström C, Wold S (2006) Multi- and Megavariate Data Analysis. Part I. Basic Principles and Applications. Umetrics Academy, Umea, Sweden

Favory JJ, Stec A, Gruber H, Rizzini L, Oravecz A, Funk M, Albert A, Cloix C, Jenkins GI, Oakeley EJ, et al (2009) Interaction of COP1 and UVR8 regulates UV-B-induced photomorphogenesis and stress acclimation in Arabidopsis. EMBO J **28:** 591–601

Foyer CH, Noctor G (2003) Redox sensing and signalling associated with reactive oxygen in chloroplasts, peroxisomes and mitochondria. Physiol Plant **119:** 355–364

Foyer CH, Noctor G (2011) Ascorbate and glutathione: the heart of the redox hub. Plant Physiol **155:** 2–18

Ghirardo A, Wright LP, Bi Z, Rosenkranz M, Pulido P, Rodríguez-Concepción M, Niinemets Ü, Brüggemann N, Gershenzon J, Schnitzler JP (2014) Metabolic flux analysis of plastidic isoprenoid biosynthesis in poplar leaves emitting and nonemitting isoprene. Plant Physiol **165:** 37–51

Goyer A (2010) Thiamine in plants: aspects of its metabolism and functions. Phytochemistry **71:** 1615–1624

Guo FQ, Crawford NM (2005) *Arabidopsis* nitric oxide synthase1 is targeted to mitochondria and protects against oxidative damage and dark-induced senescence. Plant Cell **17:** 3436–3450

Gupta KJ, Shah JK, Brotman Y, Jahnke K, Willmitzer L, Kaiser WM, Bauwe H, Igamberdiev AU (2012) Inhibition of aconitase by nitric oxide leads to induction of the alternative oxidase and to a shift of metabolism towards biosynthesis of amino acids. J Exp Bot **63:** 1773–1784

Hara MR, Agrawal N, Kim SF, Cascio MB, Fujimuro M, Ozeki Y, Takahashi M, Cheah JH, Tankou SK, Hester LD, et al (2005) S-Nitrosylated GAPDH initiates apoptotic cell death by nuclear translocation following Siah1 binding. Nat Cell Biol **7:** 665–674

Harvey CM, Li Z, Tjellström H, Blanchard GJ, Sharkey TD (2015) Concentration of isoprene in artificial and thylakoid membranes. J Bioenerg Biomembr **47:** 419–429

Hauck SM, Dietter J, Kramer RL, Hofmaier F, Zipplies JK, Amann B, Feuchtinger A, Deeg CA, Ueffing M (2010) Deciphering membrane-associated molecular processes in target tissue of autoimmune uveitis by label-free quantitative mass spectrometry. Mol Cell Proteomics **9:** 2292–2305

He Y, Tang RH, Hao Y, Stevens RD, Cook CW, Ahn SM, Jing L, Yang Z, Chen L, Guo F, et al (2004) Nitric oxide represses the Arabidopsis floral transition. Science **305:** 1968–1971

Heijde M, Ulm R (2012) UV-B photoreceptor-mediated signalling in plants. Trends Plant Sci **17:** 230–237

Holtgrefe S, Gohlke J, Starmann J, Druce S, Klocke S, Altmann B, Wojtera J, Lindermayr C, Scheibe R (2008) Regulation of plant cytosolic glyceraldehyde 3-phosphate dehydrogenase isoforms by thiol modifications. Physiol Plant **133:** 211–228

Hu J, Huang X, Chen L, Sun X, Lu C, Zhang L, Wang Y, Zuo J (2015) Site-specific nitrosoproteomic identification of endogenously S-nitrosylated proteins in Arabidopsis. Plant Physiol **167:** 1731–1746

Huang D, Zhang X, Chen ZM, Zhao Y, Shen XL (2011) The kinetics and mechanism of an aqueous phase isoprene reaction with hydroxyl radical. Atmos Chem Phys **11:** 7399–7415

Janz D, Behnke K, Schnitzler JP, Kanawati B, Schmitt-Kopplin P, Polle A (2010) Pathway analysis of the transcriptome and metabolome of salt sensitive and tolerant poplar species reveals evolutionary adaption of stress tolerance mechanisms. BMC Plant Biol **10:** 150

Jasid S, Simontacchi M, Bartoli CG, Puntarulo S (2006) Chloroplasts as a nitric oxide cellular source: effect of reactive nitrogen species on chloroplastic lipids and proteins. Plant Physiol **142:** 1246–1255

Johnson KL, Jones BJ, Bacic A, Schultz CJ (2003) The fasciclin-like arabinogalactan proteins of Arabidopsis: a multigene family of putative cell adhesion molecules. Plant Physiol **133:** 1911–1925

Kaling M, Kanawati B, Ghirardo A, Albert A, Winkler JB, Heller W, Barta C, Loreto F, Schmitt-Kopplin P, Schnitzler JP (2015) UV-B mediated metabolic rearrangements in poplar revealed by non-targeted metabolomics. Plant Cell Environ **38:** 892–904

Kasprzewska A (2003) Plant chitinases: regulation and function. Cell Mol Biol Lett **8:** 809–824

Kotak S, Larkindale J, Lee U, von Koskull-Döring P, Vierling E, Scharf KD (2007) Complexity of the heat stress response in plants. Curr Opin Plant Biol **10:** 310–316

Lane BG (2002) Oxalate, germins, and higher-plant pathogens. IUBMB Life **53:** 67–75

Latham JR, Wilson AK, Steinbrecher RA (2006) The mutational consequences of plant transformation. J Biomed Biotechnol **2006:** 25376

Lindermayr C, Durner J (2009) S-Nitrosylation in plants: pattern and function. J Proteomics **73:** 1–9

Lindermayr C, Durner J (2015) Interplay of reactive oxygen species and nitric oxide: nitric oxide coordinates reactive oxygen species homeostasis. Plant Physiol **167:** 1209–1210

Lindermayr C, Saalbach G, Durner J (2005) Proteomic identification of S-nitrosylated proteins in Arabidopsis. Plant Physiol **137:** 921–930

Loreto F, Mannozzi M, Maris C, Nascetti P, Ferranti F, Pasqualini S (2001) Ozone quenching properties of isoprene and its antioxidant role in leaves. Plant Physiol **126:** 993–1000

Loreto F, Schnitzler JP (2010) Abiotic stresses and induced BVOCs. Trends Plant Sci **15:** 154–166

Loreto F, Velikova V (2001) Isoprene produced by leaves protects the photosynthetic apparatus against ozone damage, quenches ozone products, and reduces lipid peroxidation of cellular membranes. Plant Physiol **127:** 1781–1787

Lozano-Juste J, Colom-Moreno R, León J (2011) In vivo protein tyrosine nitration in *Arabidopsis thaliana*. J Exp Bot **62:** 3501–3517

Mahalingam R, Jambunathan N, Gunjan SK, Faustin E, Weng H, Ayoubi P (2006) Analysis of oxidative signalling induced by ozone in *Arabidopsis thaliana*. Plant Cell Environ **29:** 1357–1371

Merl J, Ueffing M, Hauck SM, von Toerne C (2012) Direct comparison of MS-based label-free and SILAC quantitative proteome profiling strategies in primary retinal Müller cells. Proteomics **12:** 1902–1911

Michelet L, Zaffagnini M, Morisse S, Sparla F, Pérez-Pérez ME, Francia F, Danon A, Marchand CH, Fermani S, Trost P, et al (2013) Redox regulation of the Calvin-Benson cycle: something old, something new. Front Plant Sci **4:** 470

Mittler R (2002) Oxidative stress, antioxidants and stress tolerance. Trends Plant Sci **7:** 405–410

Moreau M, Lindermayr C, Durner J, Klessig DF (2010) NO synthesis and signaling in plants: where do we stand? Physiol Plant **138:** 372–383

Neill SJ, Desikan R, Clarke A, Hancock JT (2002) Nitric oxide is a novel component of abscisic acid signaling in stomatal guard cells. Plant Physiol **128:** 13–16

Noctor G, Mhamdi A, Foyer CH (2014) The roles of reactive oxygen metabolism in drought: not so cut and dried. Plant Physiol **164:** 1636–1648

Ortega-Galisteo AP, Rodríguez-Serrano M, Pazmiño DM, Gupta DK, Sandalio LM, Romero-Puertas MC (2012) S-Nitrosylated proteins in pea (*Pisum sativum* L.) leaf peroxisomes: changes under abiotic stress. J Exp Bot **63:** 2089–2103

Pasqualini S, Meier S, Gehring C, Madeo L, Fornaciari M, Romano B, Ederli L (2009) Ozone and nitric oxide induce cGMP-dependent and -independent transcription of defence genes in tobacco. New Phytol **181:** 860–870

Peñuelas J, Llusia J, Asensio D, Munne-Bosch S (2005) Linking isoprene with plant thermotolerance, antioxidants and monoterpene emissions. Plant Cell Environ **28:** 278–286

Portis AR Jr (2003) Rubisco activase: Rubisco's catalytic chaperone. Photosynth Res **75:** 11–27

Quideau S, Deffieux D, Douat-Casassus C, Pouységu L (2011) Plant polyphenols: chemical properties, biological activities, and synthesis. Angew Chem Int Ed Engl **50:** 586–621

Rao MV, Paliyath G, Ormrod DP (1996) Ultraviolet-B- and ozone-induced biochemical changes in antioxidant enzymes of *Arabidopsis thaliana*. Plant Physiol **110:** 125–136

Richet N, Tozo K, Afif D, Banvoy J, Legay S, Dizengremel P, Cabané M (2012) The response to daylight or continuous ozone of phenylpropanoid and lignin biosynthesis pathways in poplar differs between leaves and wood. Planta **236:** 727–737

Rizzini L, Favory JJ, Cloix C, Faggionato D, O'Hara A, Kaiserli E, Baumeister R, Schäfer E, Nagy F, Jenkins GI, et al (2011) Perception of UV-B by the Arabidopsis UVR8 protein. Science **332:** 103–106

Rodríguez-Serrano M, Romero-Puertas MC, Zabalza A, Corpas FJ, Gómez M, Del Río LA, Sandalio LM (2006) Cadmium effect on oxidative metabolism of pea (*Pisum sativum* L.) roots: imaging of reactive oxygen species and nitric oxide accumulation *in vivo*. Plant Cell Environ **29:** 1532–1544

Sandermann H, Ernst D, Heller W, Langebartels C (1998) Ozone: an abiotic elicitor of plant defence reactions. Trends Plant Sci **3:** 47–50

Seifert GJ, Blaukopf C (2010) Irritable walls: the plant extracellular matrix and signaling. Plant Physiol **153:** 467–478

Sharkey TD, Singsaas EL (1995) Why plants emit isoprene. Nature **374:** 769

Sharkey TD, Yeh S (2001) Isoprene emission from plants. Annu Rev Plant Physiol Plant Mol Biol **52:** 407–436

Shih MC, Heinrich P, Goodman HM (1991) Cloning and chromosomal mapping of nuclear genes encoding chloroplast and cytosolic glyceraldehyde-3-phosphate-dehydrogenase from *Arabidopsis thaliana*. Gene **104:** 133–138

Simontacchi M, García-Mata C, Bartoli CG, Santa-María GE, Lamattina L (2013) Nitric oxide as a key component in hormone-regulated processes. Plant Cell Rep **32:** 853–866

Singsaas EL, Lerdau M, Winter K, Sharkey TD (1997) Isoprene increases thermotolerance of isoprene-emitting species. Plant Physiol **115:** 1413–1420

Singsaas EL, Sharkey TD (2000) The effects of high temperature on isoprene synthesis in oak leaves. Plant Cell Environ **23:** 751–757

Siwko ME, Marrink SJ, de Vries AH, Kozubek A, Schoot Uiterkamp AJ, Mark AE (2007) Does isoprene protect plant membranes from thermal shock? A molecular dynamics study. Biochim Biophys Acta **1768:** 198–206

Sumiyoshi M, Nakamura A, Nakamura H, Hakata M, Ichikawa H, Hirochika H, Ishii T, Satoh S, Iwai H (2013) Increase in cellulose accumulation and improvement of saccharification by overexpression of arabinofuranosidase in rice. PLoS ONE **8:** e78269

Tanaka R, Kobayashi K, Masuda T (2011) Tetrapyrrole metabolism in *Arabidopsis thaliana*. The Arabidopsis Book **9:** e0145 DOI:10.1199/tab.0145

Tanou G, Filippou P, Belghazi M, Job D, Diamantidis G, Fotopoulos V, Molassiotis A (2012) Oxidative and nitrosative-based signaling and associated post-translational modifications orchestrate the acclimation of citrus plants to salinity stress. Plant J **72:** 585–599

Thiel S, Döhring T, Köfferlein M, Kosak A, Martin P, Seidlitz HK (1996) A phytotron for plant stress research: how far can artificial lighting compare to natural sunlight? J Plant Physiol **148:** 456–463

Tossi V, Amenta M, Lamattina L, Cassia R (2011) Nitric oxide enhances plant ultraviolet-B protection up-regulating gene expression of the phenylpropanoid biosynthetic pathway. Plant Cell Environ **34:** 909–921

Vandenabeele S, Vanderauwera S, Vuylsteke M, Rombauts S, Langebartels C, Seidlitz HK, Zabeau M, Van Montagu M, Inzé D, Van Breusegem F (2004) Catalase deficiency drastically affects gene expression induced by high light in *Arabidopsis thaliana*. Plant J **39:** 45–58

Vanzo E, Ghirardo A, Merl-Pham J, Lindermayr C, Heller W, Hauck SM, Durner J, Schnitzler JP (2014) S-Nitroso-proteome in poplar leaves in response to acute ozone stress. PLoS ONE **9:** e106886

Velikova V, Edreva A, Loreto F (2004) Endogenous isoprene protects *Phragmites australis* leaves against singlet oxygen. Physiol Plant **122:** 219–225

Velikova V, Fares S, Loreto F (2008) Isoprene and nitric oxide reduce damages in leaves exposed to oxidative stress. Plant Cell Environ **31:** 1882–1894

Velikova V, Ghirardo A, Vanzo E, Merl J, Hauck SM, Schnitzler JP (2014) Genetic manipulation of isoprene emissions in poplar plants remodels the chloroplast proteome. J Proteome Res **13:** 2005–2018

Velikova V, Loreto F (2005) On the relationship between isoprene emission and thermotolerance in Phragmites australis leaves exposed to high temperatures and during the recovery from a heat stress. Plant Cell Environ **28:** 318–327

Velikova V, Loreto F, Tsonev T, Brilli F, Edreva A (2006) Isoprene prevents the negative consequences of high temperature stress in *Platanus orientalis* leaves. Funct Plant Biol **33:** 931–940

Velikova V, Müller C, Ghirardo A, Rock TM, Aichler M, Walch A, Schmitt-Kopplin P, Schnitzler JP (2015) Knocking down of isoprene emission modifies the lipid matrix of thylakoid membranes and influences the chloroplast ultrastructure in poplar. Plant Physiol **168:** 859–870

Velikova V, Pinelli P, Pasqualini S, Reale L, Ferranti F, Loreto F (2005) Isoprene decreases the concentration of nitric oxide in leaves exposed to elevated ozone. New Phytol **166:** 419–425

Velikova V, Várkonyi Z, Szabó M, Maslenkova L, Nogues I, Kovács L, Peeva V, Busheva M, Garab G, Sharkey TD, et al (2011) Increased thermostability of thylakoid membranes in isoprene-emitting leaves probed with three biophysical techniques. Plant Physiol **157:** 905–916

Vickers CE, Gershenzon J, Lerdau MT, Loreto F (2009a) A unified mechanism of action for volatile isoprenoids in plant abiotic stress. Nat Chem Biol **5:** 283–291

Vickers CE, Possell M, Cojocariu CI, Velikova VB, Laothawornkitkul J, Ryan A, Mullineaux PM, Hewitt CN (2009b) Isoprene synthesis protects transgenic tobacco plants from oxidative stress. Plant Cell Environ **32:** 520–531

Volkov RA, Panchuk II, Mullineaux PM, Schöffl F (2006) Heat stress-induced H_2O_2 is required for effective expression of heat shock genes in Arabidopsis. Plant Mol Biol **61:** 733–746

Wang Y, Lin A, Loake GJ, Chu C (2013) H_2O_2-induced leaf cell death and the crosstalk of reactive nitric/oxygen species. J Integr Plant Biol **55:** 202–208

Way DA, Ghirardo A, Kanawati B, Esperschütz J, Monson RK, Jackson RB, Schmitt-Kopplin P, Schnitzler JP (2013) Increasing atmospheric CO_2 reduces metabolic and physiological differences between isoprene- and non-isoprene-emitting poplars. New Phytol **200:** 534–546

Way DA, Schnitzler JP, Monson RK, Jackson RB (2011) Enhanced isoprene-related tolerance of heat- and light-stressed photosynthesis at low, but not high, CO_2 concentrations. Oecologia **166:** 273–282

Wink DA, Cook JA, Pacelli R, Liebmann J, Krishna MC, Mitchell JB (1995) Nitric oxide (NO) protects against cellular damage by reactive oxygen species. Toxicol Lett **82-83:** 221–226

Wiśniewski JR, Zougman A, Nagaraj N, Mann M (2009) Universal sample preparation method for proteome analysis. Nat Methods **6:** 359–362

Xu J, Yang J, Duan X, Jiang Y, Zhang P (2014) Increased expression of native cytosolic Cu/Zn superoxide dismutase and ascorbate peroxidase improves tolerance to oxidative and chilling stresses in cassava (*Manihot esculenta* Crantz). BMC Plant Biol **14:** 208

Yang H, Mu J, Chen L, Feng J, Hu J, Li L, Zhou JM, Zuo J (2015) *S*-Nitrosylation positively regulates ascorbate peroxidase activity during plant stress responses. Plant Physiol **167:** 1604–1615

Zaffagnini M, Fermani S, Costa A, Lemaire SD, Trost P (2013) Plant cytoplasmic GAPDH: redox post-translational modifications and moonlighting properties. Front Plant Sci **4:** 450

Zaffagnini M, Michelet L, Sciabolini C, Di Giacinto N, Morisse S, Marchand CH, Trost P, Fermani S, Lemaire SD (2014) High-resolution crystal structure and redox properties of chloroplastic triosephosphate isomerase from *Chlamydomonas reinhardtii*. Mol Plant **7:** 101–120

Zimmermann G, Bäumlein H, Mock HP, Himmelbach A, Schweizer P (2006) The multigene family encoding germin-like proteins of barley: regulation and function in basal host resistance. Plant Physiol **142:** 181–192